INTERNATIONAL ATOMIC ENERGY AGENCY
UNITED NATIONS EDUCATIONAL, SCIENTIFIC AND CULTURAL ORGANIZATION

INTERNATIONAL CENTRE FOR THEORETICAL PHYSICS
34100 TRIESTE (ITALY) - P.O.B. 586 - MIRAMARE - STRADA COSTIERA 11 - TELEPHONES: 224281/2/3/4/5/6
CABLE: CENTRATOM - TELEX 460392-1

INTERNATIONAL CENTRE FOR THEORETICAL PHYSICS
- 1 APR 1985
TRIESTE

SMR/115 - 57

WINTER COLLEGE ON LASERS, ATOMIC AND MOLECULAR PHYSICS

(21 January - 22 March 1985)

INTERSTELLAR MOLECULES

P. ENCRENAZ
Meudon Observatoire
92190 Meudon
France

These are preliminary lecture notes, intended only for distribution to participants. Missing or extra copies are available from Room 229.

Introduction :

Advances in spectroscopy using large optical telescopes has led to the discovery of a fair amount of

— diffuse band in the optical region (1910 - 20) which have not been interpreted until now, and may have been identified in 1984-5 by Legon and coworkers

— narrow absorption lines (1937 - 1943) in the spectra of stars by Smith, Adams and Swings. These lines have been attributed to the CN, CH and CH^+ radicals (Herzberg, Swings), but were not used until 1968 to measure the 3K background radiation (discovered by Penzias-Wilson in 1964-5 and measured directly with the horn antenna)

Shklovsky and Townes suggested to look for OH in the late fifties, but OH was not detected until 1963 in absorption in front of Cas A. In 1969 H_2O and NH_3 were detected by Townes and his collaborators, while H_2CO, a fragile molecule in the interstellar environment, could not do better than push for a thorough search for interstellar molecules in the millimeter region of the electromagnetic spectrum. CO, CN, CH_3CN were promptly observed using a sensitive heterodyne millimeter receiver, and the field has now exploded since more than 60 molecules and 1000 transitions have been observed as of today.

A new field has been opened, which need a strong coupling between spectroscopy, collisions in atomic and molecular physics, nucleosynthesis, chemistry...

$T_{ex} = 2.8 \pm 0.1$ K
1-0

(2)

be obtained under any other reasonable assumption. While this does not prove the existence of the 3°K background, it corroborates the firmer evidence which other molecules are able to provide.

9.3.3 Optical Molecules and the 3°K Cosmic Radiation

An interesting feature of most of the light diatomic molecules observed in the interstellar medium at optical wavelengths is that their ground-state rotational energy level schemes are characterized by $E/k \sim \hbar^2/2Ik \sim 3°K$ (I is the moment of inertia of the molecule). Hence these molecules are extremely sensitive indicators of the density of the 3°K field. Figure 9.2 shows observed spectra and relevant energy levels of CH, CH^+, and CN used for sampling the 3°K field. The relative intensities of the lines shown depend on the temperature of the radiation field, assuming that the rotational level populations are in equilibrium with this field. Those lines which are not observed [R(2) in CN, R(1) in CH^+, and $R_1(1)$ in CH] indicate that only the lowest levels are populated under interstellar conditions. The energy levels show that CN samples the radiation field at 2.64 and 1.32 mm by means of the intensity ratios R(0)/R(1) and R(2)/R(1); similarly CH^+ samples the field at 0.359 mm

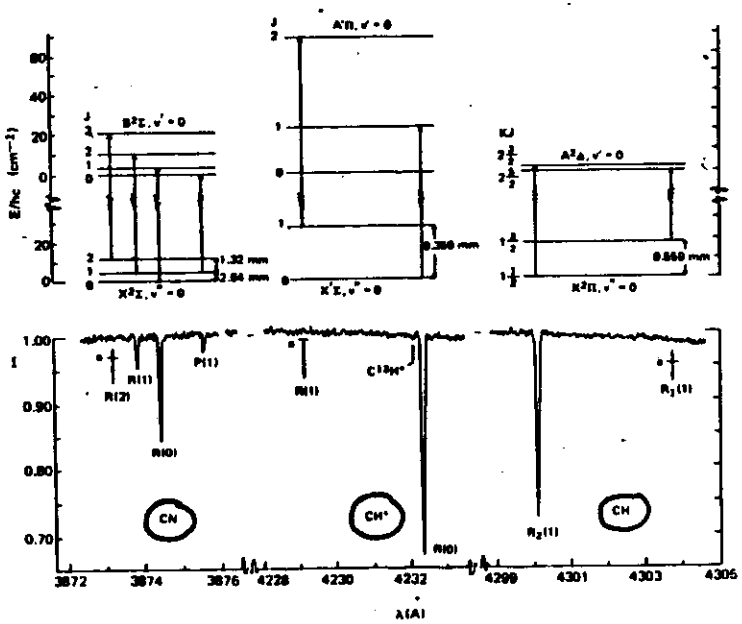

Figure 9.2 Observed spectra in the UV of the interstellar molecules CN, CH^+, and CH. The observed transitions are indicated on the energy level diagrams, as are the mm-wavelength transitions whose excitation temperatures are inferred to be that of the cosmic background radiation. (Figure reproduced by kind permission of P. Thaddeus.)

Intensités relatives des transitions élect. → températures d'excitation des niveaux de rotation

(3)

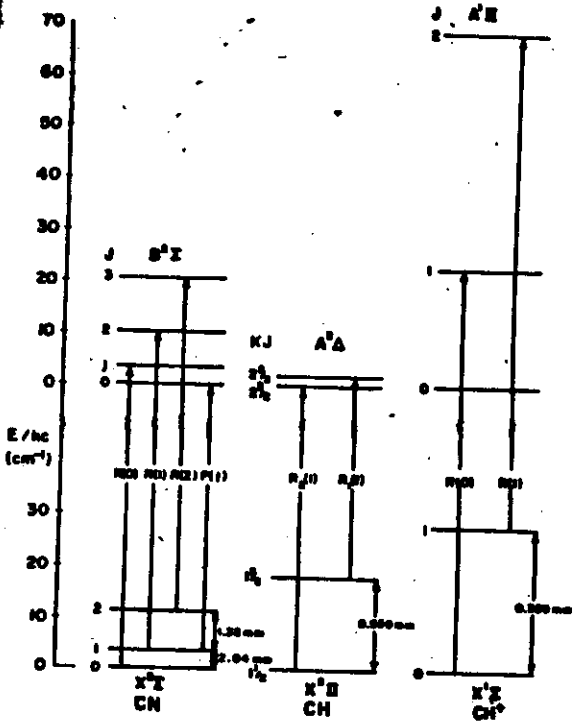

FIGURE 3. Term diagram of the strongest interstellar bands of CN, CH, and CH^+. All levels are in the lowest vibrational state.

extract from the molecular spectra extremely valuable upper limits to the radiation intensity at wavelengths even shorter than 2.64 mm. It is therefore appropriate to consider in some detail the current state of these observations, and also the theoretical analyses of local processes which show that the molecules are indeed reliable thermometers for the background radiation.

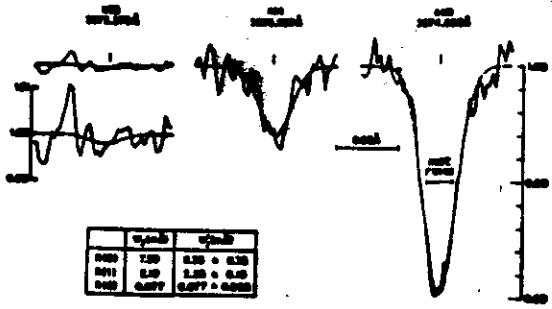

R(0)	7.59	0.35 ± 0.05
R(1)	5.89	2.35 ± 0.05
R(2)	0.077	0.077 ± 0.005

FIGURE 7. The interstellar CN lines in ζ Oph observed with a high-resolution Fabry-Perot spectrometer (Hegyi, Traub & Carleton 1972). The region of R(2) was scanned for many nights, that of R(0) and R(1) for much shorter times.

lines; we will hereon proceed as though the electronic ground state were $^2\Sigma$, and the level structure, as shown in Figure 3, that of a simple rigid rotor. Since only the two lowest rotational levels are observed to be populated in space, the fractional level populations n_0, n_1 in statistical equilibrium are determined from the rate equation

$$\frac{dn_1}{dt} = -n_1(C_{10} + A_1) + n_0 C_{01} = 0 \qquad 1.$$

where A_1 is the spontaneous radiative decay rate of the $J=1$ level,

$$A_1 = \frac{64\pi^4\nu^3\mu^2}{3hc^3} = 1.19 \times 10^{-6}\ \text{sec}^{-1} \qquad 2.$$

$\mu = 1.45 \times 10^{-18}$ cm is the CN dipole moment (Thomson & Dalby 1968) and $\nu_{10} = 1.13 \times 10^{5}$ sec^{-1}. C_{10} is the direct rate of radiative or collisional de-excitation from the $J=1$ to $J=0$ level, and C_{01} is the rate of excitation from the $J=0$ level to all others, since excitation to a level above $J=1$ is in effect immediately followed by radiative cascade to that level. Under neutral particle impact the cross sections for many-quantum transitions will be comparable to those for the $\Delta J = 1$ transitions, and C_{01} and C_{10} as defined will *not* satisfy detailed balance,

$$\frac{C_{01}}{C_{10}} = \frac{g_1}{g_0}\exp\left(-h\nu_{10}/kT_k\right) \simeq \frac{g_1}{g_0} \qquad 3.$$

where $g_0 = 1$, $g_1 = 3$, and T_k is the kinetic temperature. But since the cross sections for neutral particle excitation can only be estimated, while those for excitation

...ronic or ionic impact are rather reasonably known, and satisfy at least ...mately the selection rule $\Delta J = \pm 1$, it is permissible in the treatment of ...lines to assume that Equation 3 is satisfied. Since the optical observations ...ecular CN require

$$n_1/n_0 = (g_1/g_0)\exp\left(-h\nu_{10}/kT_R\right), \text{ with } T_R = 2.8°\text{K} \qquad 4.$$

...ation 1 may be solved for the excitation rate, yielding

$$C_{01} = (g_1/g_0)A_1 \exp\left(-h\nu_{10}/kT_R\right)\left[1 - \exp\left(-h\nu_{10}/kT_R\right)\right]^{-1}$$
$$= 6.0 \times 10^{-6}\ \text{sec}^{-1} \qquad 5.$$

...C_{01} is the rate required to account for the observed CN excitation, and T_R of ... was that obtained from 2.8°K radiation.

...The essential question we now seek to answer is whether excitation at this ... can be provided by any process in the CN cloud besides direct photo-...excitation. We shall consider collisional impact of the CN molecules with the ...l gas, either (i) with the most abundant neutral particles, presumably H atoms, ...possibly H_2 molecules, or (ii) with the residual H I electrons; or (iii) collisional impact with ions (on the odd chance that the CN molecules, or hitherto ...ed ions suggested, lie along the edge of an ionization front and are subject ...impact by ~10°K protons); and finally (iv) excitation of the rotational levels ...optical photoexcitation (resonance fluorescence). Excitation via the vibration...CN, either by collisions or infrared photons, is such a slow process that it ...not be considered.

Neutral particle impact.—Rotational excitation by H or H_2 impact is a ...collisional process dependent on short-range intermolecular forces, but by ...taken the excitation cross section cannot greatly exceed the geometrical; ...reasonable to adopt as upper limit $\sigma_{01} \sim 2 \times 10^{-15}$ cm^2. Taking $n_H = 100$ cm^{-3} ...upper limit to the density in the ζ Oph molecular cloud, and $v = 1.2 \times 10^5$ ...sec (i.e., 100°K H atoms) as an upper limit to the kinetic velocity, yields

$$C_{01} = n_H \sigma_{01} v \leq 2.2 \times 10^{-7}\ \text{sec}^{-1} \qquad 6.$$

...which falls short of Equation 5, the required rate, by a factor of about 25. The ...density of molecular hydrogen, for which the excitation cross section is comparable to that of H, is unknown in the ζ Oph cloud, but it is unlikely to exceed the ...density of the H atoms. Almost certainly, therefore, neutral particle impact is ...not the cause of the CN excitation. There is other evidence pointing to this conclusion: at the density required for such application the CO excitation temperature (Smith & Strecker 1971) and probably the optical extinction would be much ...larger than observed.

Electron impact.—Because of the long range of the Coulomb force, electron impact on H I energies is highly effective in exciting rotation of polar molecules, its rate coefficient being ~10^5 times that of neutral particles. Excitation by the ...residual electrons in an H I region is for this reason the least process which ...comes closest to accounting for the 2.8° CN excitation, and it accordingly de-

④

⑤

This molecule, whose list is given in table I, are made of the most abundant elements (H, C, N, O, S, Si, Fe), and their isotopic molecules are also detected (H/D , $^{12}C/^{13}C$, $^{14}N/^{15}N$, $^{16}O/^{17}O/^{18}O$, $^{28}Si/^{29}Si/^{30}Si$, $^{32}S/^{33}S/^{34}S$ .....

Before we try to understand the impact of these discoveries on astronomy, I will go back to their simple principles for the excitation of these molecules, and I will explain how this can be of practical interest for galactic (H I).

[redacted]

Table of the most abundant elements

H	3.18	10^{10}
C	1.18	10^{7}
N	3.7	10^{6}
O	2.15	10^{7}
S	5	10^{5}
Si		10^{6}
Cl	5.7	10^{3}
Fe	8.3	10^{5}

Isotopic Ratios (solar neighborhood)

H/D	5×10^5
$^{12}C/^{13}C/^{14}C$	89 / radioactive
$^{14}N/^{15}N$	280
$^{16}O/^{17}O/^{18}O$	3000 / 500
$^{32}S/^{33}S/^{34}S$	100 / 20
$^{28}Si/^{29}Si/^{30}Si$	20 / 25
$^{35}Cl/^{37}Cl$	4 / 1

1 LES MOLÉCULES INTERSTELLAIRES OU CIRCUMSTELLAIRES CONNUES À CE JOUR

A] Atomic Neutral Hydrogen : HI

① The 21 cm line was discovered in 1951. This transition connects two hyperfine levels of atomic hydrogen with either parallel or antiparallel spins of the proton and electron

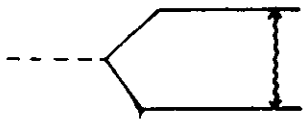

The spontaneous transition rate $A_{21} = 2.84 \times 10^{-15}\ s^{-1}$ is exceedingly small (magnetic dipole transition). The life time of the excited atom is therefore of the order of 10^7 years.

A] ② Line formation :

Let $I(\nu)$ be the specific intensity of the radiation field at the frequency ν: $I(\nu) = \frac{c}{4\pi} u(\nu)$ ($u(\nu)$ in erg cm^{-3} Hz^{-1} = spectral density energy)

= erg cm^{-2} s^{-1} st^{-1} Hz^{-1}

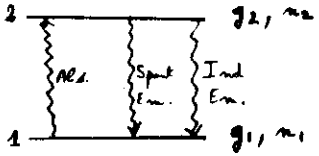

By definition, the Einstein coefficient are given by: $g_1 B_{12} = g_2 B_{21}$

$$B_{21} = \frac{c^2}{2h\nu^3} A_{21}$$

with $\mathcal{N}_{1\to 2} = n_1 B_{12} I(\nu)$

$\mathcal{N}_{2\to 1} = n_2 (A_{21} + B_{21} I(\nu))$

(number of transition 1→2 and 2→1 per unit time and unit volume).

If $I(\nu) = 0$, the spontaneous life time gives $\tau_2 \sim \frac{1}{A_{21}}$ (coupling with the fluctuation of the vacuum).

The variation of $I(\nu)$ along an elementary path ds can therefore be written $\frac{dI(\nu)}{ds} = \frac{1}{\delta\nu} \times \frac{h\nu}{4\pi} \times (\mathcal{N}_{2\to 1} - \mathcal{N}_{1\to 2})$ as all photons are redistributed in a frequency interval $\delta\nu$.

The equation is usually written $\frac{dI(\nu)}{ds} = j(\nu) - \kappa(\nu) I(\nu)$

$j(\nu)$ in erg cm^{-3} s^{-1} st^{-1} Hz^{-1}

$\kappa(\nu)$ in cm^{-1}

By definition the optical depth is $d\tau(\nu) = -\kappa(\nu) ds$

$$\kappa(\nu) = \frac{1}{\delta\nu} \frac{h\nu}{4\pi} n_1 \frac{g_2}{g_1} \frac{c^2}{h\nu^3} A_{21} \left(1 - \frac{n_2}{n_1} \frac{g_1}{g_2}\right)$$

Or, if we introduce the excitation temperature T_{ex} such that

$$\frac{n_2}{n_1} = \frac{g_2}{g_1} \exp\left(-\frac{h\nu}{k T_{ex}}\right)$$

$$\kappa(\nu) = \frac{1}{\delta\nu} \frac{h\nu}{4\pi} n_1 \frac{g_2}{g_1} \frac{c^2}{2h\nu^3} \left(1 - \exp\frac{-h\nu}{k T_{ex}}\right)$$

or, if $h\nu \ll k T_{ex}$

$$\boxed{\kappa(\nu) = \frac{1}{\delta\nu} \frac{h\nu}{4\pi} n_1 B_{12} \frac{h\nu}{k T_{ex}}}$$

③ Population of the levels 1 and 2:

The 2 levels system is supposed to interact only with the radiation field (characterized by $I(\nu)$) and with particles (inelastic collisions). These particles (H, H_2, ions...) have a Maxwellian Distribution of kinetic temperature T_K.

$$f(u)\,du = \left(\frac{m_r}{2kT_K}\right)^{3/2} e^{-\frac{m_r u^2}{2kT_K}} 4\pi u^2\,du$$

m_r = reduced mass

The population of levels 1 and 2 change with time, but we will assume that the equilibrium is reached before $I(\nu)$ and T_K change

significantly: $\frac{dn_1}{dt} = \frac{dn_2}{dt} = 0$

$$n_1 B_{12} I(\nu) + n_1 C_{12} = n_2 B_{21} I(\nu) + n_2 A_{21} + n_2 C_{21}$$

C_{12} (and C_{21}) are the probabilities of collisional excitation, and de-excitation)

It can be shown that the Maxwellian hypothesis imply $n_1 C_{12} = n_2 C_{21}$ and that $T_{ex} = T_K$. We have thermodynamic equilibrium.

[R] if $\frac{dI_\nu}{ds} = 0$ (system isolated from all external radiation), then

$$I(\nu) = \frac{j(\nu)}{\kappa(\nu)} = \frac{2h\nu^3}{c^2} \frac{1}{\left[\exp\frac{h\nu}{kT} - 1\right]} \quad \text{(Black body spectrum)}$$

$$\frac{n_2}{n_1} = \frac{B_{12} I(\nu) + C_{12}}{B_{21} I(\nu) + A_{21} + C_{21}}$$

Two interesting limiting cases : $- C_{21} >> A_{21}\left[1 + I(\nu)\frac{c^2}{2h\nu^3}\right]$ and then $T_{ex} = T_K$

$- C_{21} << A_{21}\left[1 + I(\nu)\frac{c^2}{2h\nu^3}\right]$

$T_{ex} = T_R$

④ 21 cm transition: $\frac{h\nu}{k} = .07\ K$

$T_K \sim 100\ K$

$T_R = 2.8\ K$ (cosmological background)

$\frac{c^2}{2h\nu^3} I(\nu) = 43.6$

$\nu = 9.8 \times 10^3 \sqrt{T_K}$ cm s^{-1}

$\sigma_{HH} \sim 10^{-15}$ cm^2

Collisions are dominant if $n > 10^{-3}$ cm^{-3}. This is ALWAYS the case

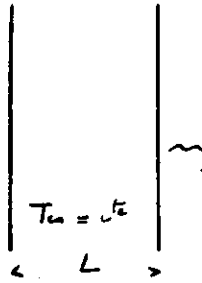

A photon of frequency ν will interact only with the cloud of HI atom having the velocity v such that $\frac{v}{c} = \frac{\nu - \nu_0}{\nu_0}$ (within the natural width of the line).

The Kramer equation can be solved and gives

$$I(\nu) = I_0(\nu) \exp\left[-\tau(\nu)\right] + B(\nu)\left[T_{ex}\right]\left[1 - \exp - \tau(\nu)\right]$$

$$\tau(\nu) = \int_L \kappa(\nu)\, ds$$

$$B_\nu(T_{ex}) = \frac{2h\nu^3}{c^2}\left[\exp\left(\frac{h\nu}{kT_{ex}}\right) - 1\right]^{-1} = \frac{j(\nu)}{\kappa(\nu)}$$

By definition the brightness temperature T_B is the temperature of a black body having $T(\nu)$ at frequency ν. Using the Rayleigh - Jeans approximation ($B_\nu(T) = \frac{2kT\nu^2}{c^2}$), the equation becomes

$$T_B(\nu) = T_{B_0}(\nu) e^{-\tau(\nu)} + T_{ex}(\nu)\left(1 - e^{-\tau(\nu)}\right)$$

$$\tau(\nu) = 5.48\ 10^{-19} \frac{N_{HI}\, P(v)}{T_{ex}} \quad (P(v) \text{ is the probability of the HI atom to have a projected velocity between } v \text{ and } v + \delta v).$$

Observations: - on a cloud at two frequencies

$$T_B^{on}(\nu) = T_{ex}\,\tau(\nu) + T_{B_0}(\nu)$$

$$T_B^{off}(\nu') \sim T_{B_0}(\nu') \sim T_{B_0}(\nu)$$

$$\Delta T_B \sim 5.48\ 10^{-19} N_{HI}\, P(v)$$

Si on somme sur la raie

$$\int_{raie} \Delta T_B(\nu)\, d\nu = 5.48 \times 10^{-19} N_{HI}$$

$$N_{HI} = 1.8 \times 10^{18} \int_{raie} \Delta T_B\, dv \quad \text{cm}^{-2}$$

– on and off a cloud at the same frequency

$$T_B^{on} = T_{B_0} e^{-\tau(\nu)} + T_{ex}\left(1 - e^{-\tau(\nu)}\right)$$

$$T_B^{off} = T_{ex}\left(1 - e^{-\tau(\nu)}\right)$$

$$\Delta T_B(\nu) = T_{B_0}\left[1 - \tau(\nu)\right] \Rightarrow \text{mesure de } \tau(\nu)$$

The last case is the use of pulsars for measuring $\tau(\nu)$ and the distance of these objects.

B] The case of simple molecules:

If you lower the temperature of a cloud of neutral hydrogen, its density will increase and you will form molecules. The most abundant of these molecules, H_2, cannot be detected by its emission spectrum. But CO, the second most abundant, has only a simple spectrum that it is quite straightforward to understand it completly:

a) linear molecule: $E(J)/h = B_0 J(J+1) - D_J\left[J(J+1)\right]^2$

The centrifugal distortion is 10^{-4} to 10^{-6} smaller than the rotational term.

$$\nu(J, J-1) \simeq 2 B_0 J$$

	B_0 (MHz)	D KHz	μ Debye	J	$A_{J,J-1}$ (s^{-1})
^{12}CO	57 636	183	0.11	1	6×10^{-8}
^{13}CS	24 496	40	1.95	3	6×10^{-5}
HCO^+	44 594	.09	4.07	1	5×10^{-5}

$$A_{J,J-1} = \frac{64\pi^4\mu^2}{3hc^3}\nu^3\frac{J}{2J+1}$$

$$A_{J,J-1} = 9.3\ 10^{-20}\ B_0^3\mu^2\frac{J^4}{2J+1}\ (s^{-1})\ \frac{B_0}{\mu}\ \frac{MHz}{debye}\ (10^{-19}\ cgs)$$

Certaines molécules ne seront excitées que dans des milieux très denses

If we follow the same reasoning than in A], we obtain

$$g_{J-1}\ C_{J-1,J} = g_J\ C_{J,J-1}\ \exp\left(-\frac{h\nu}{kT_K}\right)$$

$$\sigma_{01}(CO) \sim 2\times10^{-15}\ cm^2$$

$$R_{J,J-1} = \langle \sigma_{J,J-1} v_{H_2} \rangle$$

CO – H_2 10 K

J	ϕ	1	2	3
ϕ	–	.393	.263	.011
1	.176	–	.193	.07
2	.276	.351	–	.09
3	.046	.00		–

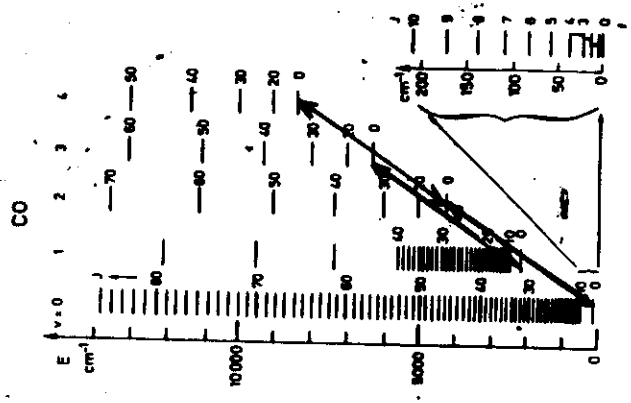

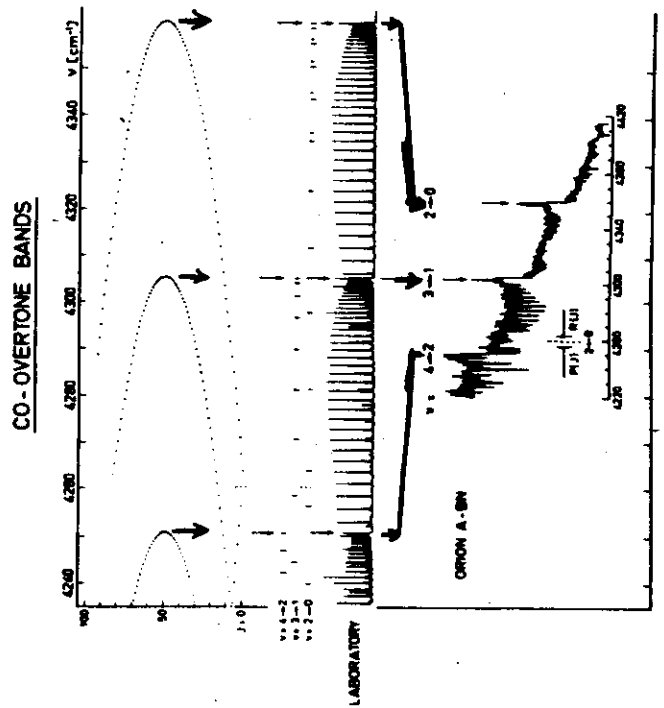

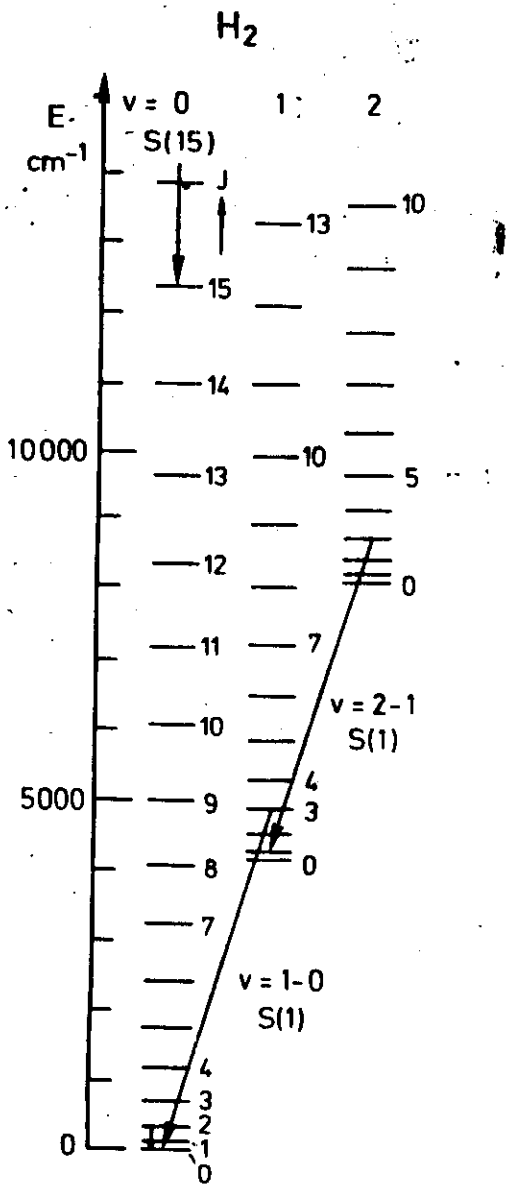

ENERGY LEVELS AND LOW J-TRANSITIONS OF

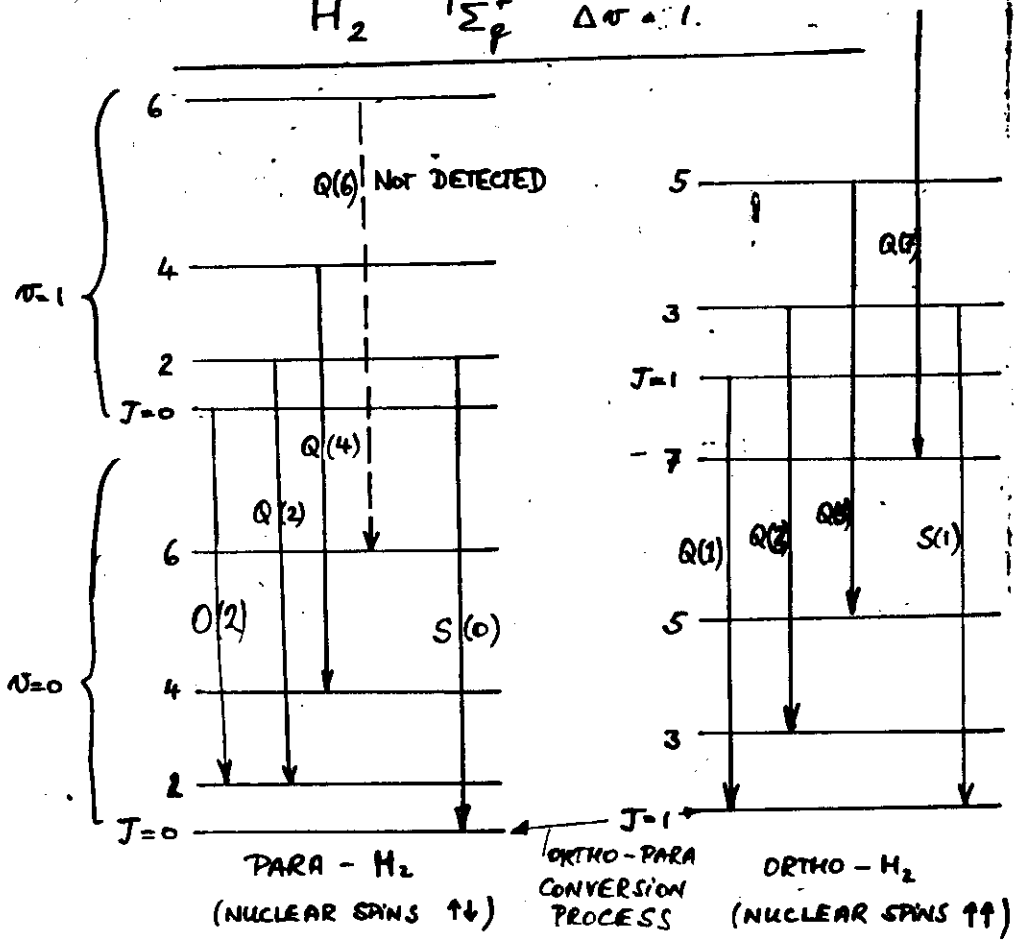

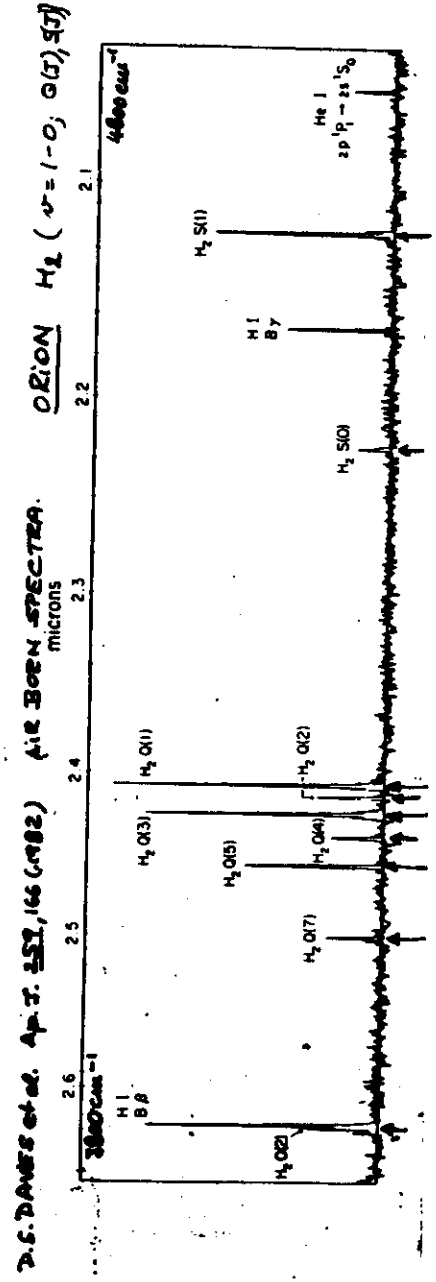

RADIATION FROM NEUTRAL CLOUDS

MAINLY MOLECULAR TRANSITIONS

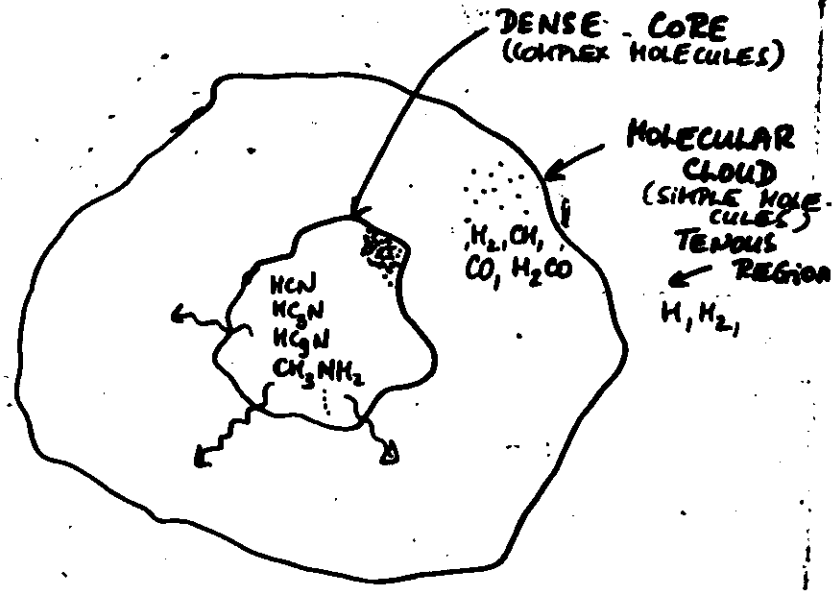

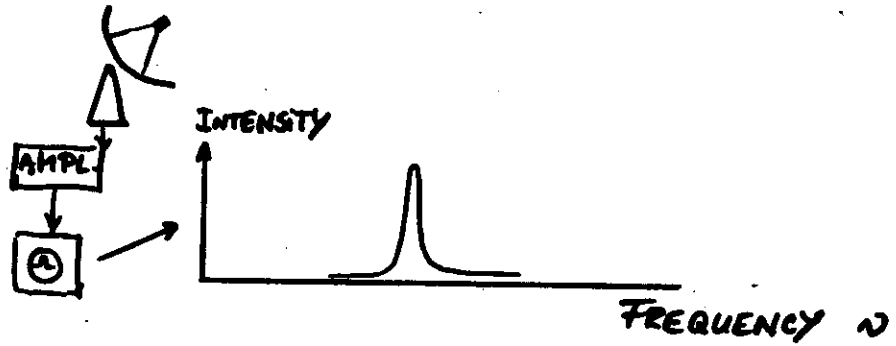

LINE BRIGHTNESS TEMPERATURE

η = beam filling

τ = optical depth

$$T_B = \eta \left(J_\nu(T_{ex}) - J_\nu(T_{BG})\right)(1 - e^{-\tau})$$

ENERGY INPUT

Background RADIATION T_{BG} → MOLECULAR LINE T_B →

ABSORPTION LINES

1. $T_{BG} = 2.7\,K$ →

2. RADIO CONTINUUM (HII-REGIONS) →

3. IR-CONTINUUM (HOT DUST) →

$T_{ex} < T_{BG}$: ABSORPTION LINES

1. H_2CO, 2cm, 6cm
   $T_{ex} < 2.7\,K$
   ANOMALOUS COOLING

2. e.g. NH_3 in DR21, SgrB2

3. CO ABSORPTION IN ORION
   $v = 2 \leftarrow 0;\ 1 \leftarrow 0$

4. Self Absorption (MANY MOLECULES + RADICALS)

$$J_\nu(T) = \frac{h\nu}{k}\left\{\exp\left(-\frac{h\nu}{kT}\right)\right.$$

EXCITATION AND LINE FORMATION.

MOLECULAR GAS (H_2)
T_{kin}
MOLECULAR TRANSITION
T_{ex}

excitation temperature T_{ex}

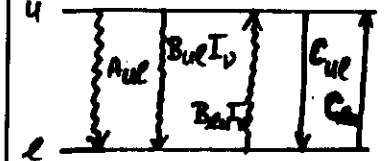

COLLISIONAL EXCITATION RATE:

$$C_{ul} = n_{gas} \langle \sigma_{ul} v \rangle_{T_{kin}}$$

RADIATION FIELD:

$$I_\nu = \langle I_{BG} e^{-\tau} \rangle + \langle I_{Dust} \rangle$$

$$n_u(A_{ul} + B_{ul} I_\nu + C_{ul}) = n_l (B_{lu} I_\nu + C_{lu}) \quad (1)$$

$$C_{lu} = C_{ul}\left(\frac{g_u}{g_l} \exp\left(-\frac{h\nu}{kT_{kin}}\right)\right) \quad (2)$$

$$\frac{n_u}{n_l} = \frac{g_u}{g_l} \exp\left(-\frac{h\nu}{kT_{ex}}\right) \quad (3)$$

LIMITING CASES

$T_{ex} \sim T_{bg}$ ($\tau \ll 1$; $C \ll A$)

$T_{ex} \sim T_{kin}$ ($C \gg A$)

$T_{ex} > T_{BG}$ EMISSION LINES

FROM GAS AT $T \sim 10 - 3000\,K$

EXCITATION CAUSED BY

GENERAL AND LOCAL ENERGY SOURCES

1. COLD CLOUDS (2.7 K, C.R., gen. stellar rad. background)

$T_{kin} \sim 10\,K$; $n_{H_2} \sim 10^4\,cm^{-3}$

Example: Taurus cloudlets, ...

CO, NH_3, H_2CO, Radicals + Ions

(Note: possibly surrounded by warmer shells).

2. WARM CLOUDS: environment of embedded stars, IR sources

$T_{kin} \sim 5 - 50\,K$; $n_{H_2} \sim 10^5 - 10^7\,cm^{-3}$

(cloud close to star $\sim$ 1pc)

Example: W51, S140 (LTE-excitation)

DR 21, S106 (non LTE-excitation)

CS, NH_3, HCN, (RADICALS AND IONS

3. HOT CENTERS: environment very close to embedded star $\sim$ 0.1pc

$T_{kin} \sim 100 - 600\,K$; $n_{H_2} \sim 10^7\,cm^{-3} - 10^9$

Examples: ... NH_3 in Orion ($\sim$ 200 K)

... CO high velocity wings (Orion, S140, ...

... CO vibrational/high rotational transitions in Orion $\sim$ 600 K.

4. MOLECULAR SHOCK FRONTS:

in regions of active star formation.

$T_{kin} \sim 1000\,K - 3000\,K$

Examples:

... H_2 rotation-vibration line emission. ($\sim$ 1500 K)

... CO Overtone Bandhead Emission ($\sim$ 3500 K)

... NH_3 $(J,K) > (9,9)$

Note:

The HOT CENTERS and MOLECULAR SHOCK FRONTS are associated with high velocity gas flows.

5. CIRCUMSTELLAR SOURCES

Mass-outflow from evolved stars

$T_{kin} \sim 100 - 1000\,K$

$n_{H_2} \sim 10^4 - 10^6\,cm^{-3}$

CO, HCN, ... RADICALS AND IONS

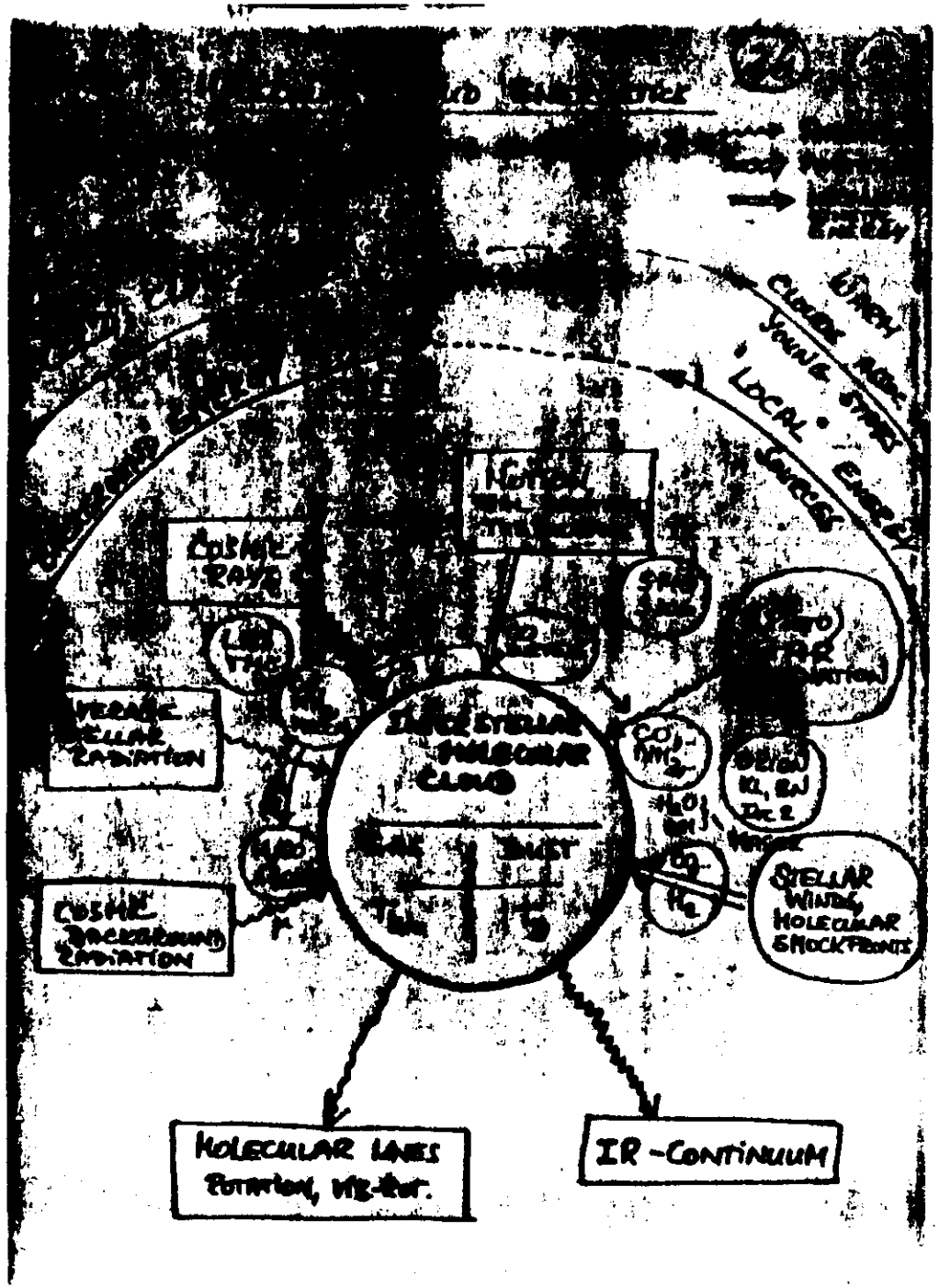

c) Non linear molecule :

The energy spectrum is not so straightforward. For a precise calculation, see Townes and Schallow (Microwave Spectroscopy) or Gordy and Cook (new edition). *

In the case of ammonia, the doublet of the transition (inversion) helps us for measuring the physical parameters of the cloud in which ammonia is excited.

There also, the computation of the potential NH_3, H_2 at low temperature is necessary to understand the physics of the collision.

The case of formaldehyde, a particularly well known molecule in the laboratory has prompted many efforts to observe its many transitions (6 cm to 1 mm). Being fairly abundant and ubiquitous, it really is a milestone in our study of the interstellar medium.

I would like to mention the identification of SiC_2 by Thaddeus and coworkers as a beautiful piece of molecular spectroscopy.

* $\frac{1}{h} E(J,K) = BJ(J+1) + (A-B)K^2$

$K = -J, -J+1, \ldots +J$

$\Delta J = 0, \pm 1 \qquad \Delta K = 0$

ON

ion of the interstellar H_2O
5_{23} has indicated a maser
me molecular process must
sively or to depopulate the
it.

. LEVELS

) that either the 6_{16} or the
ll other levels; there seems
they happened to be very
ulate excessively a group of
-A levels) or depopulate a
23 level. We divide many
Group-A levels which are
levels which are composed
levels with $K_c = J$ in which
the C-axis. The justification
by spontaneous emission is
of H_2O sorted according to
the bottom of each column
hat spontaneous emissions
ting from the $J_{0,J}$ and $J_{1,J}$
ively, which also belong to
the weaker transitions with
fore if once molecules are
energy the only radiative
3 transitions. In particular
is the first way out of the
es Group-B levels there will
ncreased induced emission
roup-B levels via the maser

levels must be one of the
ie pumping and relaxation
ociation process. Normally
ional anomalies because it
for example. Townes and
we wish to examine the

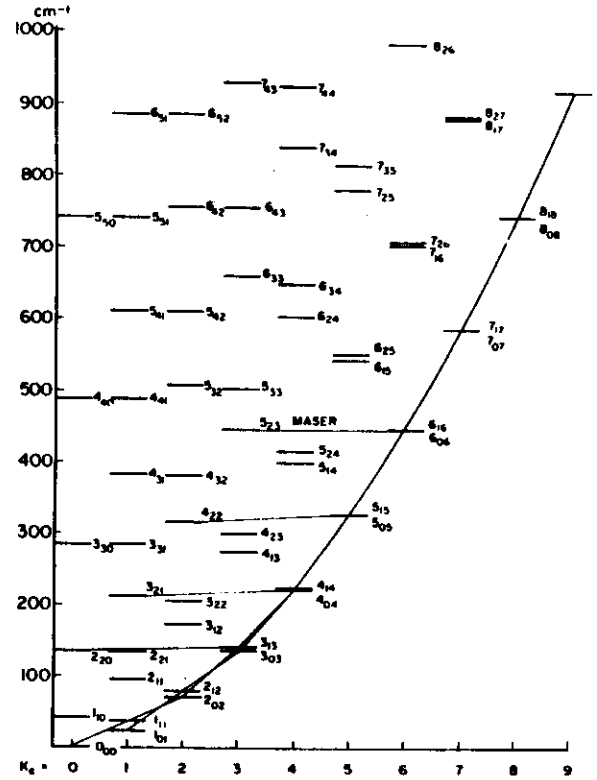

1. Rotational energy levels of H_2O molecules sorted out with K_c. The Group-A levels are composed of $J_{0,J}$ and $J_{1,J}$ levels which lie at the bottom of each column for a given K_c. The lines connecting various levels indicate spontaneous emission of the H_2O molecules. It should be noted that if molecules in Group-A levels relax from high energy levels the maser transition $6_{16} \rightarrow 5_{23}$ is the first connection between the Group-A and Group-B levels. Therefore if some molecular process depletes molecules in the Group-B levels there will be an inverted population between the 6_{16} and the 5_{23} levels.

gy, as $^4\Sigma^-$, $^2\Sigma^-$ and $^4\Pi$.
mon (1968), makes the
peratures much greater
) and H atoms close to
$^+$ curve. The switching
rms $X^2\Pi$ OH. Second,
requires about 1000°K,
the pre-association rate
ssociation (the inverse
don and Kopp (1971),
$^4\Sigma^-$ states. This rate is
er A states. These rates
ping, as seen in Figure
cable to the maximum

vapor maser. Collisions
to about J=5 if the
re is likely to be about
in either of the maser
out 10^{-4} or 10^{-5} times
n A-coefficients and
igher rotational levels,
temperatures to about
e noted that the 6_{16}
23 level. The observed
tical depths. Because
depths for the various
large. The resonance
appears to make the
of 5_{23} (lower maser
quate to pump these
cause collisions across
lizing effect. Infrared
asterisks leads to
l, making population
vel can be shown to

naldehyde that was
e-strength shown in
d 1_{10}. However, the
$)_{00}$" level does not

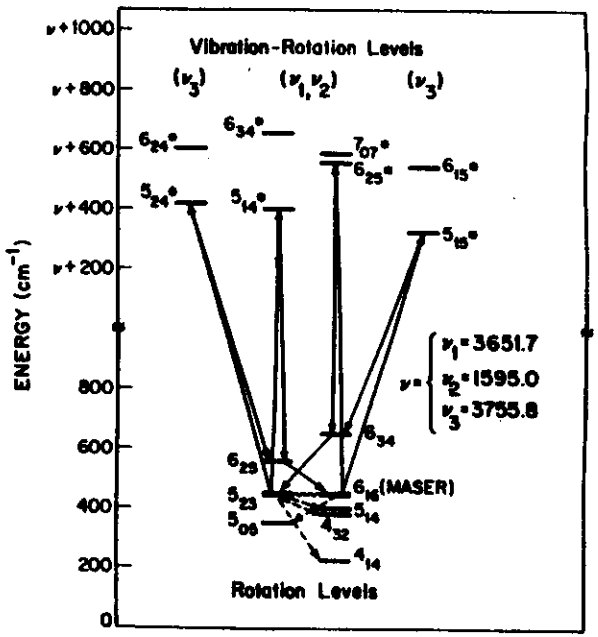

INFRARED PUMPING OF 22.2 GHz H_2O MASER

7. Rotation and vibration-rotation levels involved in infrared pumping of H_2O maser (22.2 GHz). The lower rotational levels (many not shown) are in nearly-thermal equilibrium because of collisions.

(28)

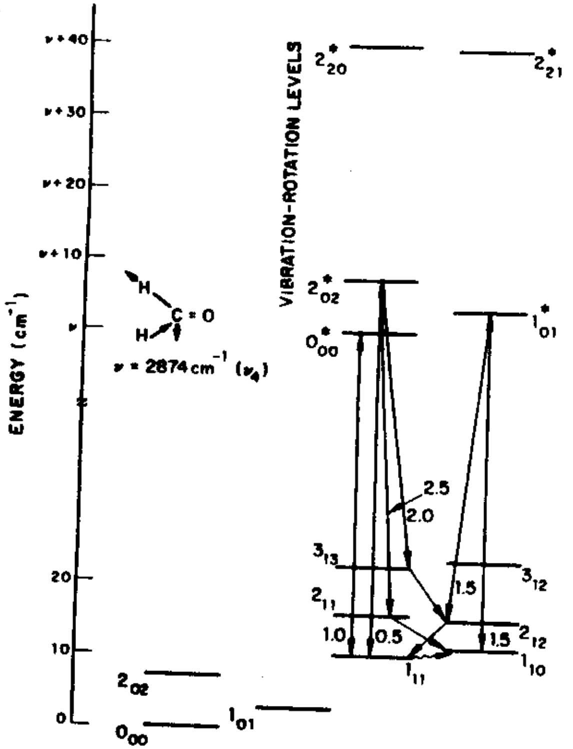

8. Lower rotation and vibration-rotation levels involved in infrared pumping of formaldehyde (ortho) anti-maser at 6-, 2- and 1-cm wavelengths (J = 1, 2 and 3 doublets, respectively).

(29)

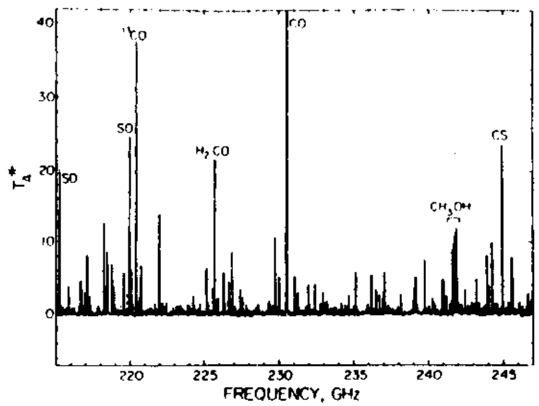

FIG. 1.—Spectrum of Orion A from 215 to 247 GHz. Data were obtained with a typical receiver noise temperature of 300 K (SSB) and backend coverage of 527 MHz. The original spectral resolution was 1.03 MHz (1.3 km s^{-1}). Spectral resolution in this plot is degraded by about a factor of 10.

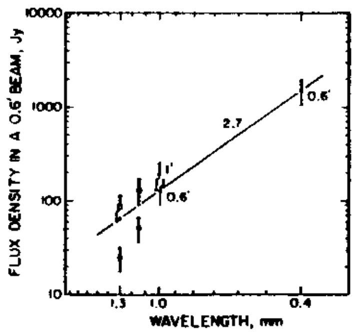

FIG. 2.—Broad-band and spectral line flux densities in a 0.6 beam centered on BN. Open circles show the line fluxes measured by Sutton *et al.* (1984) and Blake *et al.* (1984). Open boxes indicate the total broad-band fluxes measured simultaneously. Crosses represent the broad-band fluxes of Keene, Hildebrand, and Whitcomb (1982) and Elias *et al.* (1978), the latter both for a 1' beam and corrected for a 0.6 beam. Plus sign represents the extrapolation of these short wavelength measurements to 1.3 mm.

However, some additional uncertainties were introduced since the spectral line system was not well optimized for continuum observations. The measured broad-band flux was 86 Jy at 1.3 mm with an uncertainty of about ±15% on top of an overall calibration error of ±20%.

This value for the broad-band flux can be compared with the various values in the published literature. The 400 μm emission from the core of Orion A has been measured and mapped with 0.6 resolution by Keene, Hildebrand, and Whitcomb (1982). They show that the submillimeter emission consists of an extended component plus two major compact sources. The flux density at BN is 1500 Jy within a 0.6 beam, with an overall calibration uncertainty of ±30%. Previously, the 1 mm emission from Orion was measured by Westbrook *et al.* (1976) and recalibrated by Elias *et al.* (1978). They derived a flux density of 188 Jy in a 1' beam. Assuming that the 1 mm emission has the same spatial distribution as the 400 μm emission, it is possible to estimate the 1 mm flux density in a 0.6 beam by using the mapping data of Keene, Hildebrand, and Whitcomb (1982). The result is an estimated flux density of 128 Jy for the smaller beam. Combined with the 400 μm result, this implies a spectral index of 2.7 between 0.4 mm and 1 mm. This is similar to but smaller than the spectral index estimated by Elias *et al.* (1978). Extrapolating with this spectral index to 1.3 mm, the wavelength of the spectral line observations, gives a flux density of 63 Jy in a 0.6 beam. The various broad-band fluxes are plotted in Figure 2. Comparison with the line flux indicates that 30%–40% of the total flux may be accounted for as line emission. This, however, is a lower limit since the line flux is based only on those lines stronger than 0.2 K.

III. DISCUSSION

a) Extrapolation to Weaker Lines

The calculations above have considered only those lines strong enough to be individually detected, i.e., those with peak antenna temperatures stronger than about 0.2 K. There will be a large number of weaker lines present which cannot be seen because of the noise level in the spectrum and because of the overlapping of stronger lines. Even at the 0.2 K level there are large regions of the spectrum in which the baseline cannot be clearly seen due to the overlapping wings of strong lines.

Some weaker lines can be predicted with some precision because they involve transitions with weaker matrix elements or are between more highly excited states of well-known species. But the general problem of predicting the number of

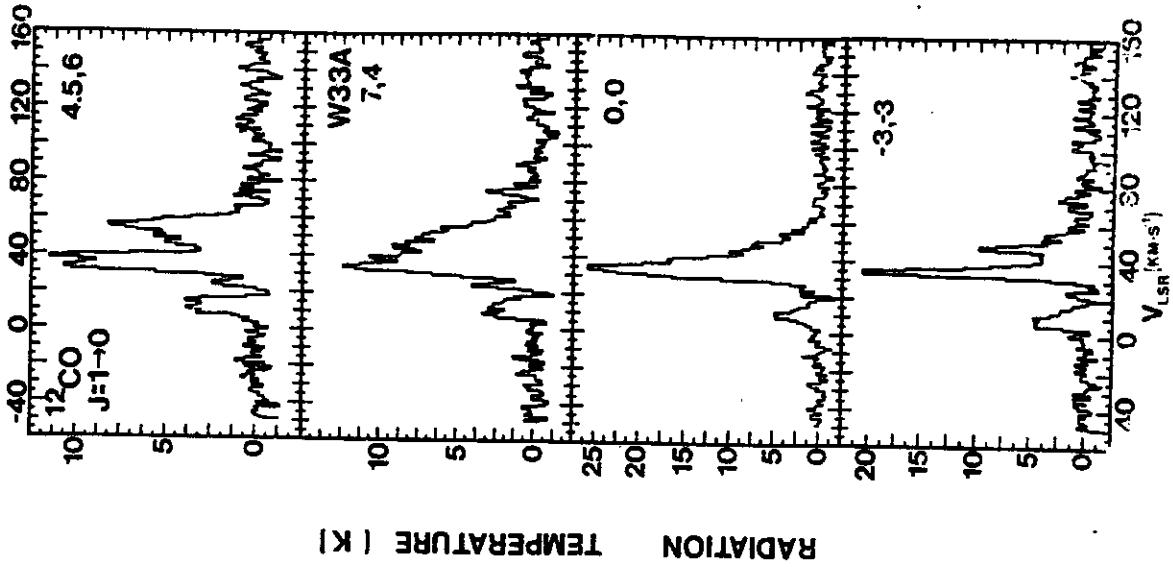

Figure 1

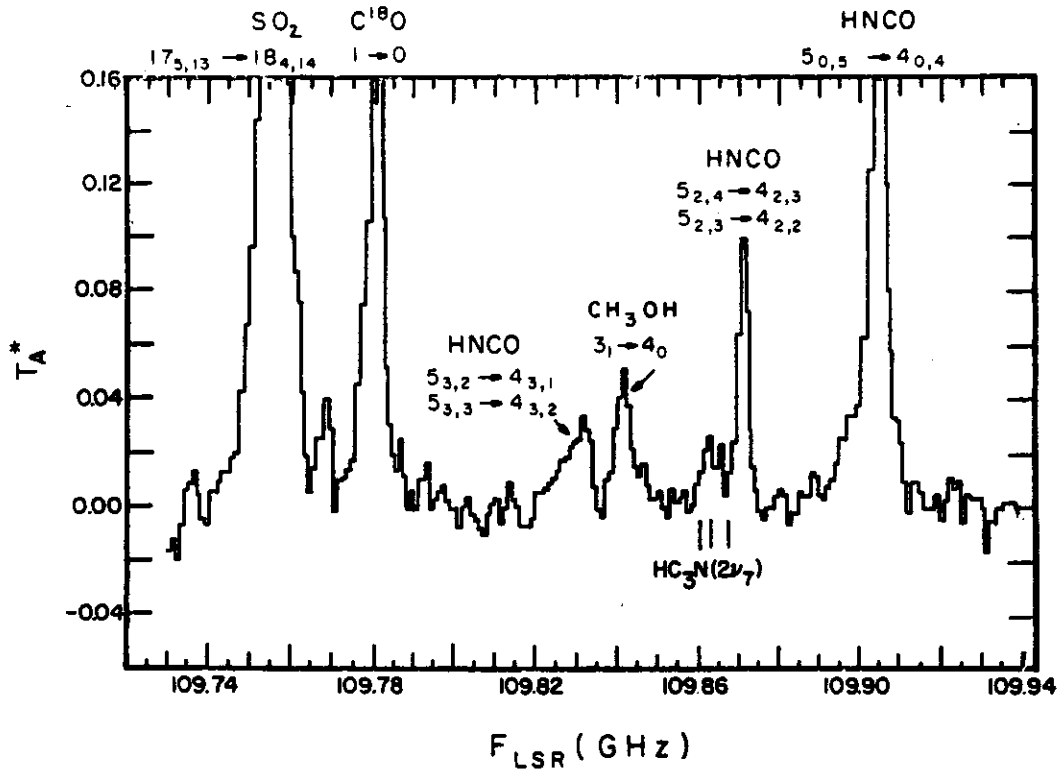

FIGURE 1

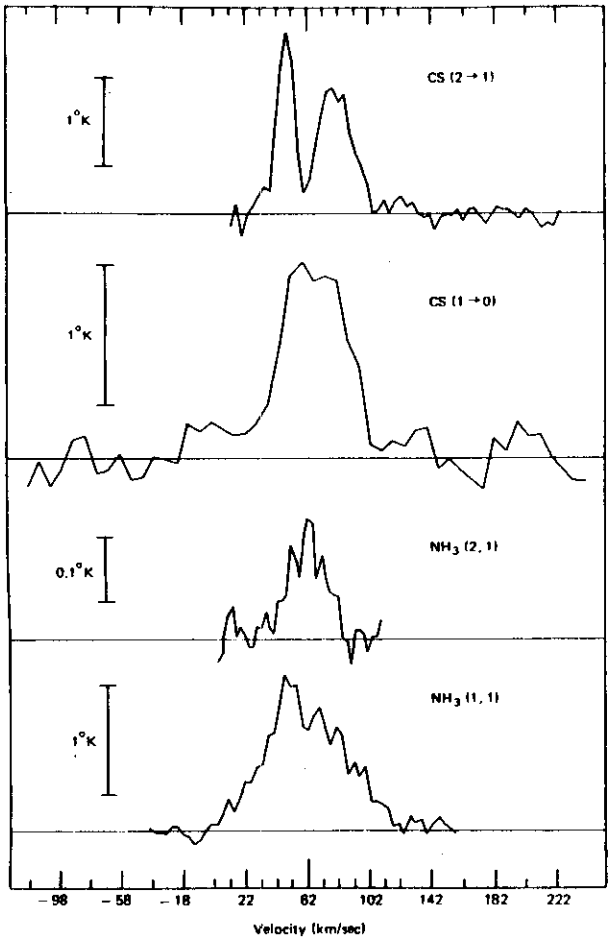

Figure 9.1 Spectra of NH_3 and CS in the Sgr B2 molecular source. The observation of the (2,1) line of NH_3 indicates that densities as high as 10^8 cm^{-3} may exist in the core of the source. The striking difference in the 2 → 1 and 1 → 0 lines of CS indicates that the Sgr B2 source may consist of two separate clouds or density condensations.

the line width. A secondary peak occurs in the HCO^+ line profile at a velocity of 5 km s^{-1} and at the velocity of the peak of the $H^{13}CO^+$ the HCO^+ line profile reaches a minimum at nearly the zero level. Even more severe self-absorption occurs near ρ Oph B2. In Figure 4, at a

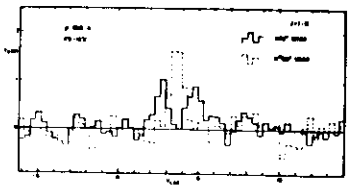

Figure 4. The J=1-0 HCO^+ and $H^{13}CO^+$ line profiles toward a position 2' east of ρ Oph B2.

position 2'E of B2, the $H^{13}CO^+$ has twice the intensity of the HCO^+ and is centered between the two HCO^+ peaks. At the core of ρ Oph B2 we have obtained high resolution line profiles of the J=1-0 HCO^+ and $H^{13}CO^+$, J=3-2 HCO^+ and J=2-1, 3-2, 4-3 DCO^+ transitions (Fig 5). While different velocity resolutions were used for some of the lines, adjacent channels have been summed so that all of the final spectra have about the same resolution. All of the DCO^+ lines occur at 4.1 km s^{-1} and show no evidence of additional components. The HCO^+ lines, in contrast, show considerable structure. Both the J=1-0 and J=3-2 HCO^+ profiles have absorption dips at slightly less than 4 km s^{-1}. The J=1-0 $H^{13}CO^+$ also seems to have a very narrow deep dip which occurs at the velocity of the J=3-2 HCO^+ peak. This is the only position which shows two component structure in the $H^{13}CO^+$ line profiles. All positions adjacent to ρ Oph B2 show only a single component, although at 2'N of B2 this component is shifted to a lower velocity, 2.9 km s^{-1}. Without further observations it can not be determined whether the $H^{13}CO^+$ is self-absorbed or two separate cloud components are present. The strength of the J=3-2 HCO^+ and J=1-0 $H^{13}CO^+$ at ρ Oph B2 relative to the J=1-0 HCO^+ reveals that the latter is self-absorbed. The shift to a lower velocity also occurs in the DCO^+ lines at the position 2'N of ρ Oph B2.

5. PHYSICAL CONDITIONS WITHIN THE DENSE CORES

The observations reveal that there are a number of identifiable condensations within the ρ Oph cloud and that there is considerable variation in the physical conditions from region to region. In the J=1-0 HCO^+ map several peaks, to the

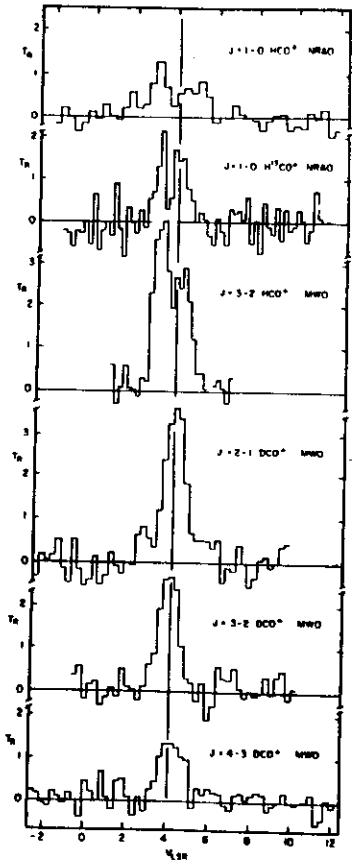

Figure 5. The line profiles of HCO^+, $H^{13}CO^+$ and DCO^+ lines toward ρ Oph B2.

H_2CO energy levels

(34)

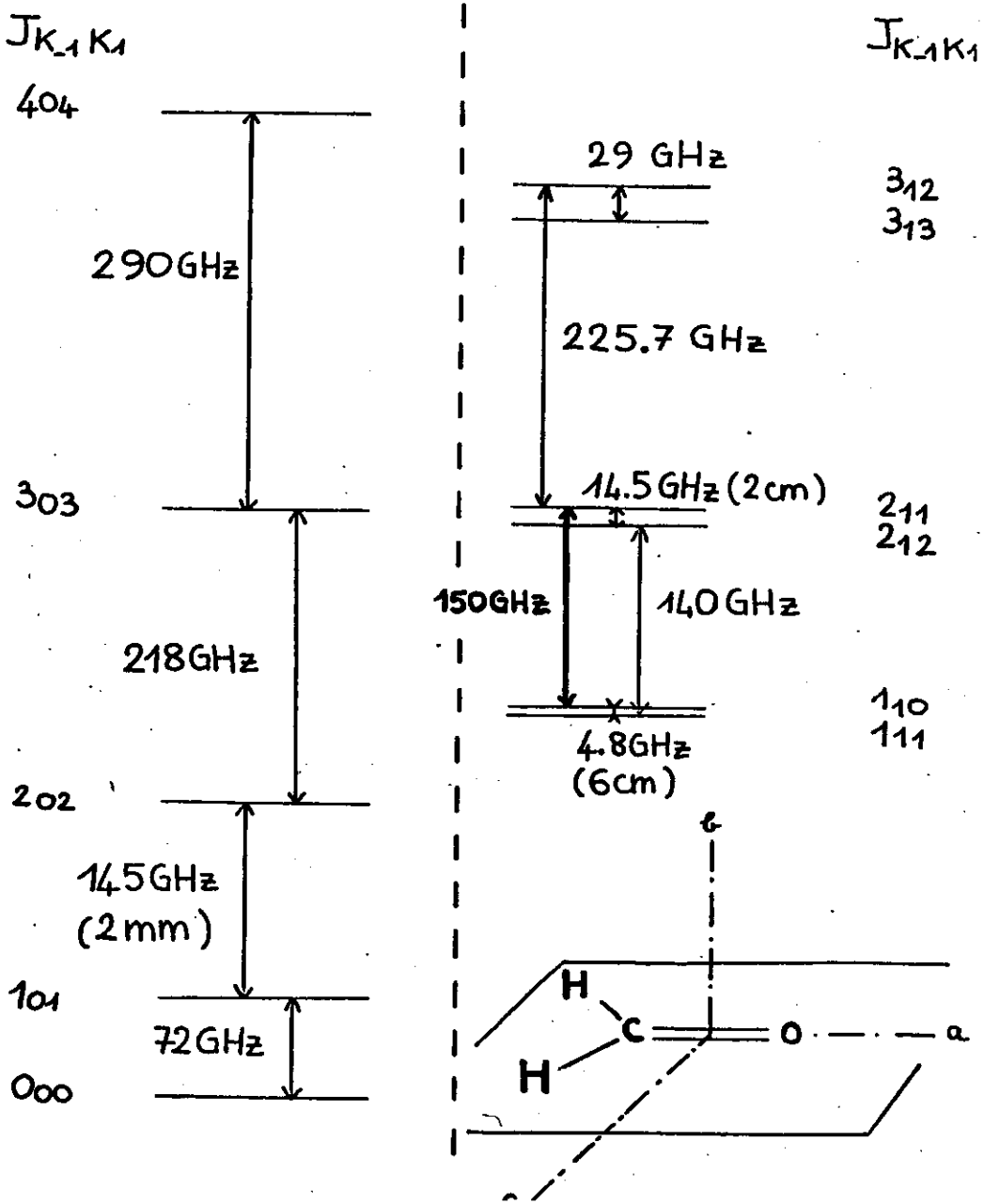

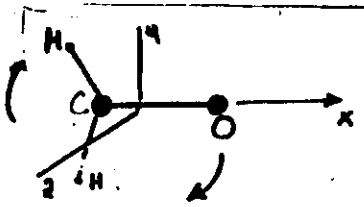

(35)

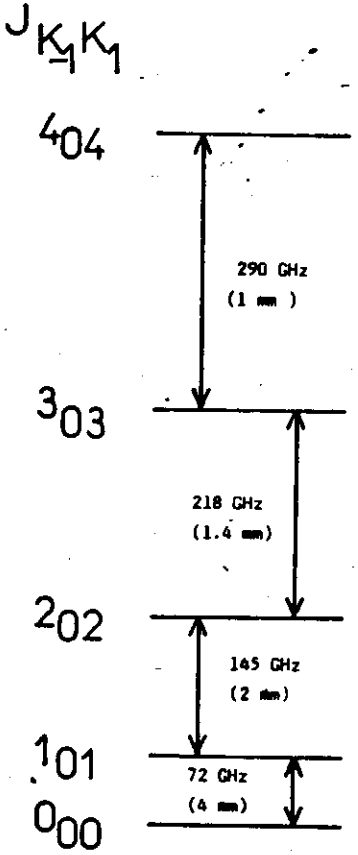

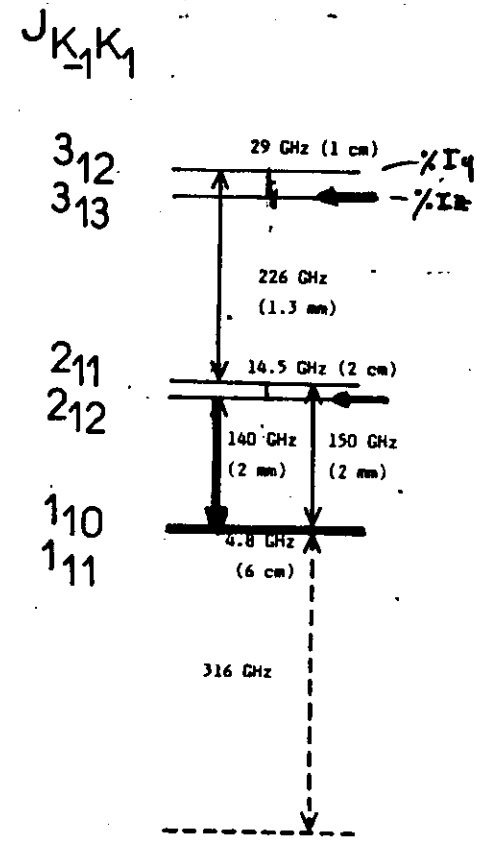

H_2CO

Figure B3 : Les premiers niveaux de rotation de la molécule H_2CO ainsi que les fréquences et les longueurs d'onde des transitions rotationnelles observées dans les nuages moléculaires. La flèche en pointillés indique la différence d'énergie entre le fondamental de l'orthoformaldéhyde et celui du paraformaldéhyde.

WHY MEASURE $[o]/[p]$? H_2CO (36)

$$[o]/[p] = 3 \times F(T)$$

In The Laboratory $F(T) \equiv 1$

In the Interstellar Medium; $F(T)$ depends

of - H_2CO chemistry

- T of the clouds

For every transition observed, plot of

$T_B = f(n_{H_2}, N_{H_2CO})$. In Principle

you can measure (n_{H_2}, N_{H_2CO}).

(37)

Pour chaque transition observ

on trace la courbe $T_B = f(n_{H_2}, N$

En principe, il y a intersectio

et on mesure (n_{H_2}, N_{H_2CO}).

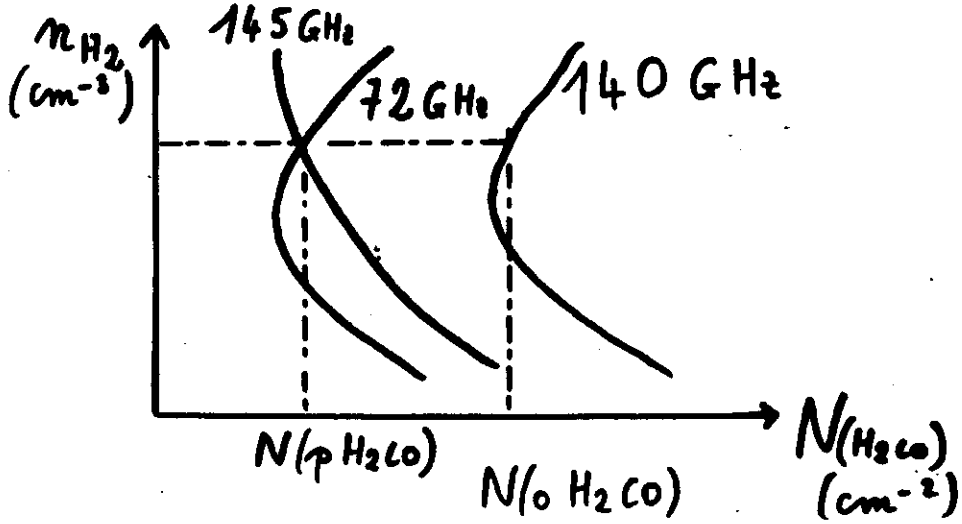

ANT TEMP DEGREES
-2.00
0.00
2.00
4.00
6.00
H2CO 145 GHZ ORIA
-20.0
0.0
20.0
40.0

38

ANTENNA TEMPERATURE
-2.00
0.00
2.00
H2CO 150 GHZ ORIA
-20.0
0.0
20.0
40.0

39

DIFFICULTIES:

- optical depth of H_2CO 2 mm line
- fragmentation of the cloud
- size of the beam at different frequencies
- is chemical equilibrium reached?

CONCLUSIONS:

- $[O]/[P] \sim 3$ in ORION
- $[O]/[P] \sim 1.5$ in Low temperature clouds
- fragments needed in ORION
- isotopic ratio smaller in ORION ($^{12}C/^{13}C$)

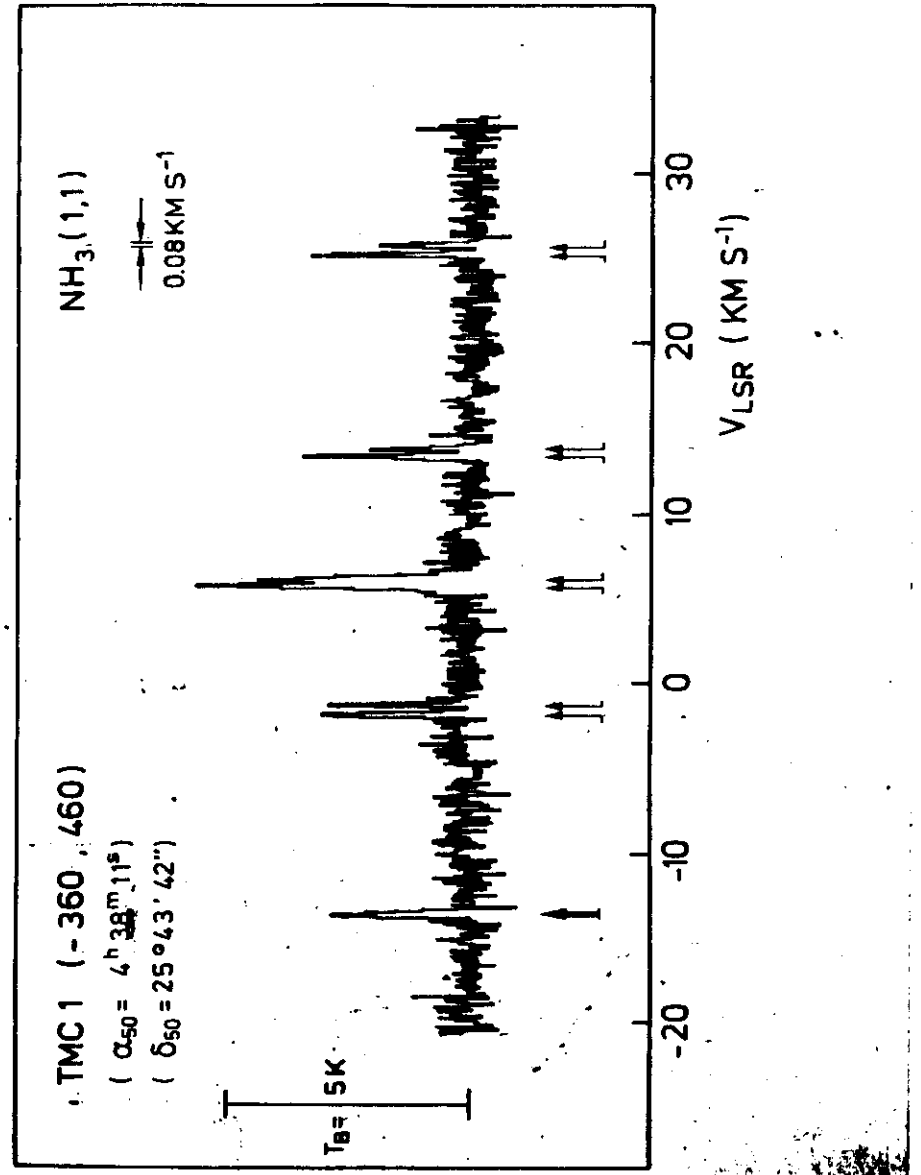

c) The broadening of the line profiles:

In molecular clouds, the linewidth is determined by Doppler-broadening: – gaussian thermal broadening
– turbulent
– systematic motions

Only in the case of rotation, it appears that turbulence the main cause of broadening, and that the line clouds are supra-thermal, but still gaussian

If you look in the same cloud two different transitions for two different molecules, you may be able to measure the kinetic temperature of the cloud Tk:

In L 183 $\Delta v_1 = 0.21$ km/s for NH_3

$\Delta v_2 = 0.11$ km/s for HC_3N

$$T_{kin} = \frac{\Delta v_1^2 - \Delta v_2^2}{8 \ln 2 k} \frac{m_1 m_2}{m_2 - m_1} = 8.4 \text{ K}$$

Another cause of broadening is the one of large optical depth (see Modern Aspects of Microwave Spectroscopy by CHANTRY for a detailed analysis).

CAUTION: reliability of this method may be questionable see IRC +10216 spectra of different molecules !!

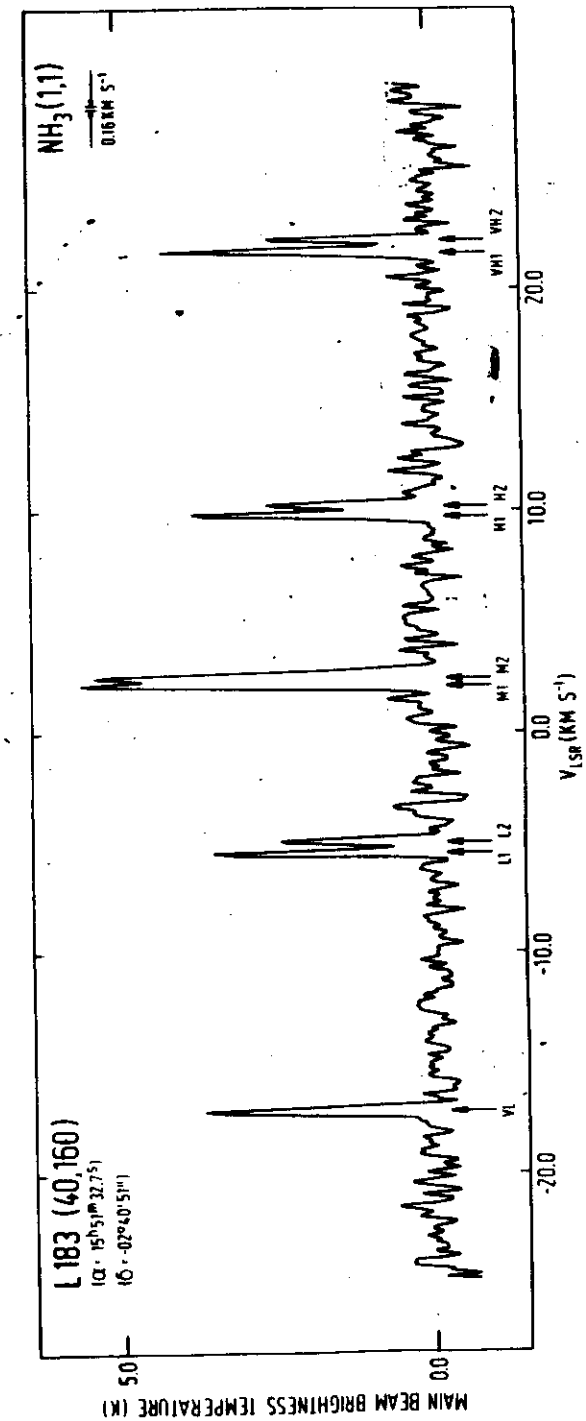

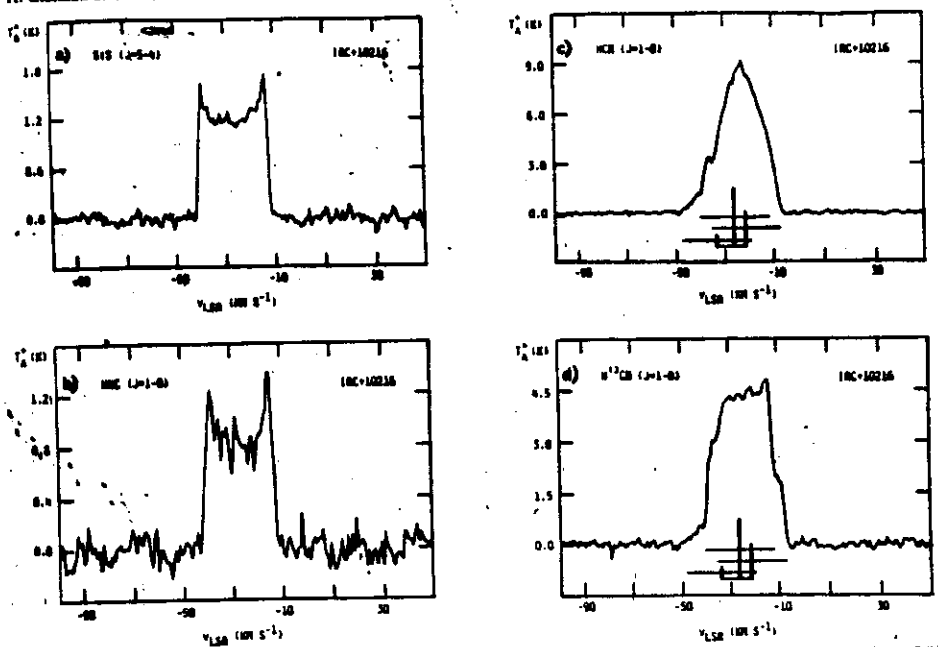

Fig. 4. a SiS ($J=5-4$), b HNC ($J=1-0$), c HCN ($J=1-0$), and d $H^{13}CN$ ($J=1-0$) spectra of IRC +10216 (velocity resolution ~0.85 km s^{-1}). The center velocities, the full widths at zero power (determined from the stellar velocity and the gas expansion velocity derived in Sect. V), and the LTE-ratios for the three quadrupole components of HCN and $H^{13}CN$ have been entered

An upper limit (3σ) may be placed on the SiO ($v=1$, $J=2-1$) *(iii)* HNC, $J=1-0$, *Fig. 4b*

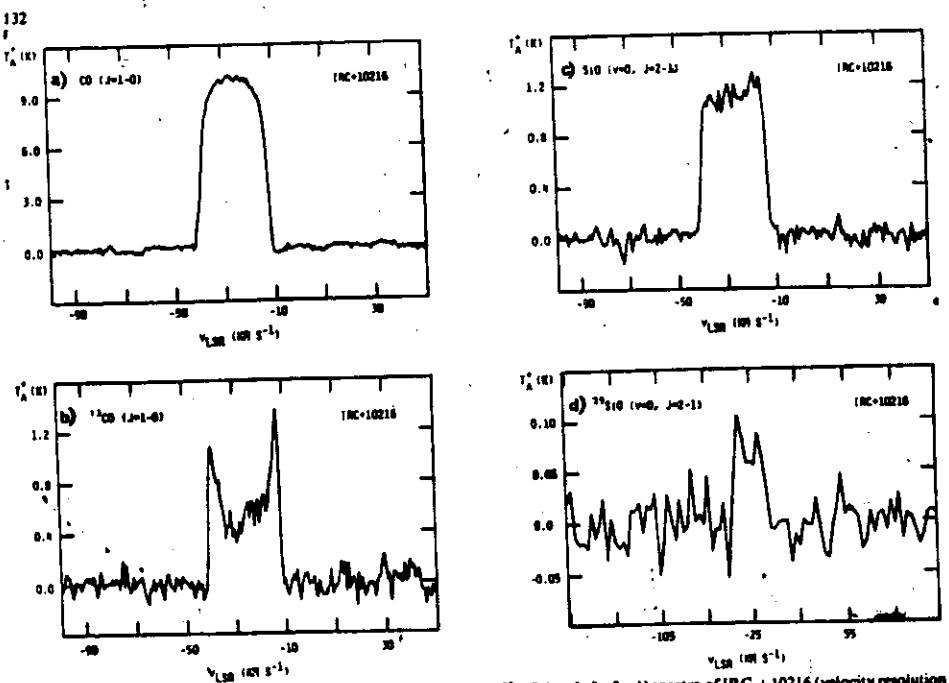

Fig. 3. a CO ($J=1-0$), b ^{13}CO ($J=1-0$), c SiO ($v=0$, $J=2-1$), and d ^{29}SiO ($v=0$, $J=2-1$) spectra of IRC +10216 (velocity resolution ~0.67 km s^{-1} in a and b, 0.86 km s^{-1} in c, and 3.5 km s^{-1} in d)

where

$\gamma_{l,u}=2(\ln 2)^{1/2}R_{l,u}/B$.

We have in Fig. 2 also entered values for $T_A^*(v=v_e)/T_A^*(v=0)$

(i) CO *and* ^{13}CO, $J=1-0$, *Fig. 3a and b*

The ^{13}CO and CO profiles are excellent examples of spatially resolved optically thin and thick emissions. The antenna tempera-

(44)

(45)

300 K

200 K

100 K

3_{31} 3_{30}

3_{21}

3_{22}

3_{12}

3_{03} 3_{13}

2_{20}

2_{21}

2_{11}

2_{12}

2_{02}

1_{10}

1_{11}

1_{01}

0_{00}

H_2D^+

EXCITATION AND LINE FORMATION

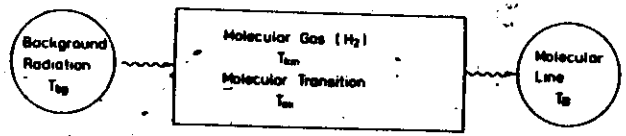

Excitation Temperature T_{ex}

two level model (rate equilibrium)

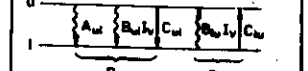

$n_u(A_{ul} + B_{ul}J_\nu + C_{ul}) = n_l(B_{lu}J_\nu + C_{lu})$ (I)

A_{ul}, B_{ul}, B_{lu} = Einstein Coefficients

$J_\nu = \langle I_{bg} e^{-\tau} \rangle < \langle I_{ul} \rangle$ = radiation field

$C_{lu} = n_{gas} \langle \sigma_{lu} v \rangle_{T_{kin}}$ = collisional excitation rate

C_{ul} and C_{lu} are related by

$$C_{lu} = C_{ul} \left(\frac{g_u}{g_l} \exp\left(-\frac{h\nu}{kT_{kin}}\right) \right) \quad (II)$$

T_{ex} is defined by

$$\frac{n_u}{n_l} = \frac{g_u}{g_l} \exp\left(-\frac{h\nu}{kT_{ex}}\right) \quad (III)$$

In general, T_{ex} is calculated by substituting (III) and (II) in (I)

important limiting cases

$C \gg A$ $\quad T_{ex} \sim T_{kin}$

$C \ll A$, $\tau \ll 1$ $\quad T_{ex} \sim T_{bg}$

Line Brightness Temperature T_B

$$T_B = \eta \{ J_\nu(T_{bg}) - J_\nu(T_{bg}) \} (1 - e^{-\tau})$$

$$J_\nu(T) = \frac{h\nu}{k} \left(\exp\left(-\frac{h\nu}{kT}\right) - 1 \right)^{-1}$$

$\sim T$ (if $kT \gg h\nu$)

η = beam filling factor

τ = optical depth

important limiting cases

$T_{ex} \gg T_{bg}$, $\tau \gg 1$

$T_B \sim \eta J_\nu(T_{ex}) \sim \eta T_{ex}$

$T_{ex} \ll T_{bg}$, $\tau \ll 1$

$T_B \sim \eta J_\nu(T_{ex}) \tau \sim \eta T_{ex} \tau \sim N$

(proportional to column density)

Absorption lines

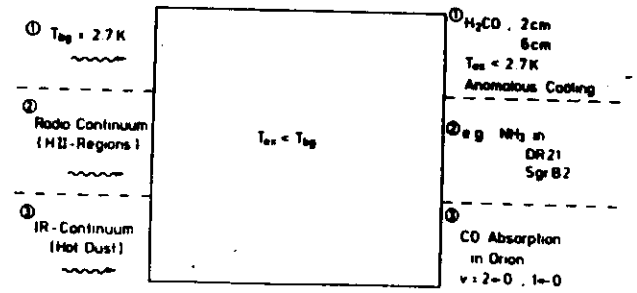

Interstellar chemistry:

The density is so small and the temperature so low that the chemistry of the interstellar molecules has little to do with the laboratory chemistry. The binary collisions between atoms, or between atom and ions will therefore be the building blocks of the heavy molecules. But certain types of collisions do necessitate a third body (dust grain for example) to recoil the energy: this is the case for the most important one (molecular hydrogen).

$$H + H \rightarrow H_2 + \Delta E$$

ΔE must be absorbed by a 3rd body

In the dense molecular clouds, opaque to the U.V. radiation field, the COSMIC RAYS do ionize the major constituents and produce H^+, H_2^+, He^+ which will react rapidly with CO, H_2 ... to build more complex molecules.

$$H_2^+ + H_2 \longrightarrow H_3^+ + H$$
$$H_3^+ + CO \rightarrow HCO^+ + H_2$$

Some of the possible schemes are presented in the following transparencies. The models used for predicting the abundances of the light molecules are close to the measured abundances. However H_2 and H_2CO do not fit this scheme and must be fabricated on dust grains (physisorption on the surface of the interstellar grains).

One of the major successes of gas phase chemistry has been the prediction of the enrichment in deuterium of deuterated molecules: I will elaborate on DCO^+ and ^{13}CO respectively:

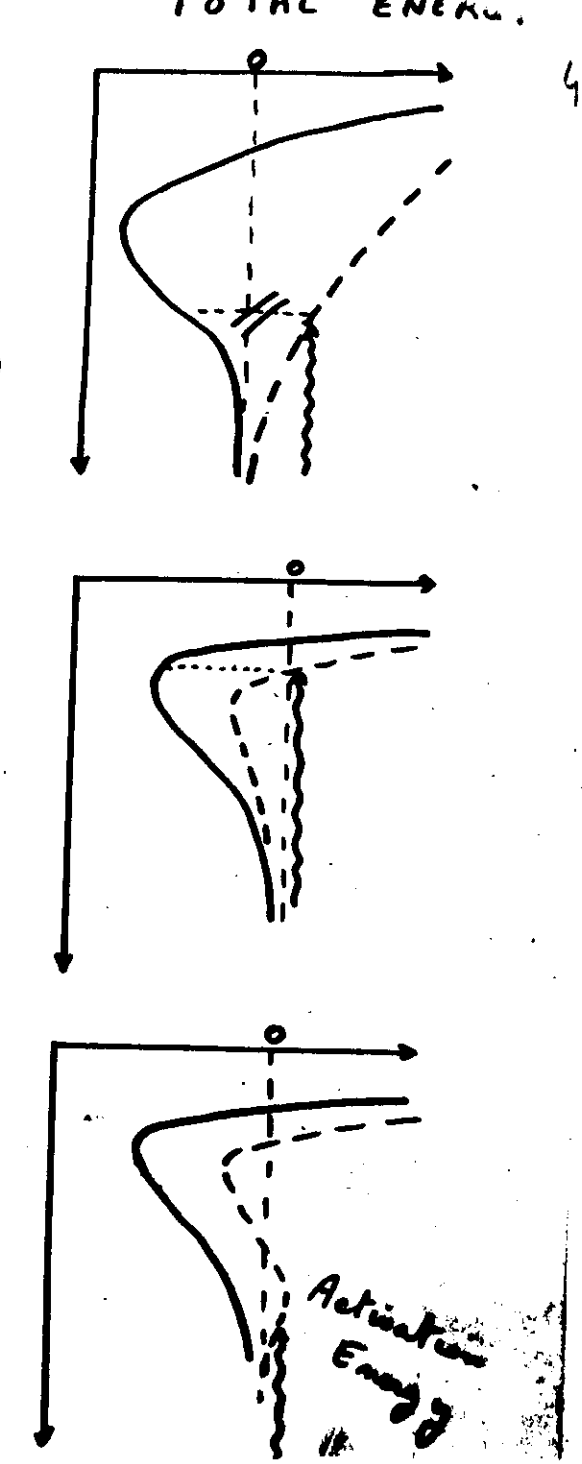

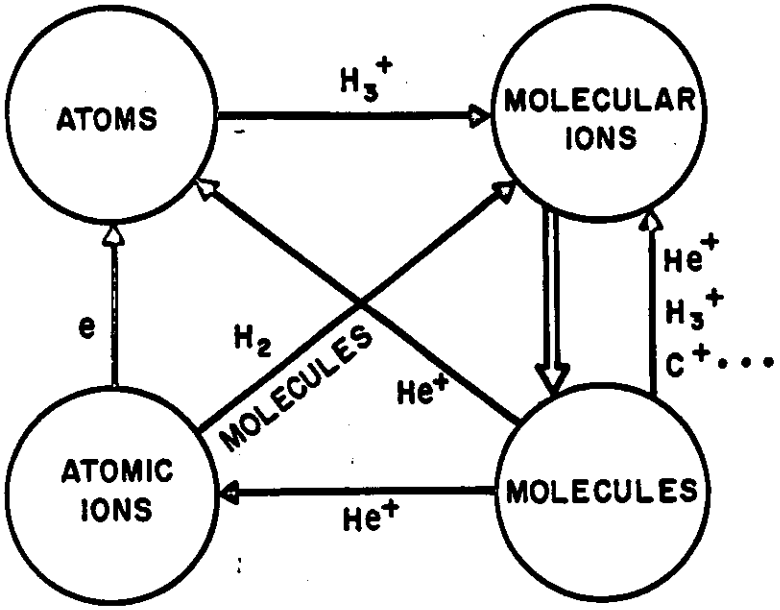
ATOMS
H_3^+
MOLECULAR IONS
e
H_2
MOLECULES
He^+
He^+
H_3^+
$C^+ \cdots$
ATOMIC IONS
MOLECULES
He^+

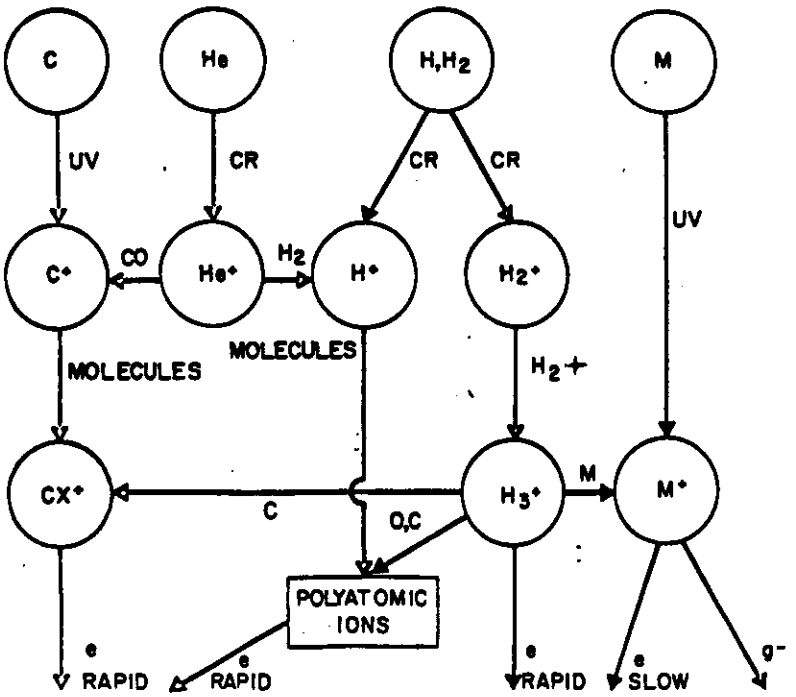
C
He
H,H_2
M
UV
CR
CR
CR
UV
C^+
CO
He^+
H_2
H^+
H_2^+
MOLECULES
MOLECULES
H_2^+
CX^+
C
O,C
H_3^+
M
M^+
POLYATOMIC IONS
e RAPID
e RAPID
e RAPID
e SLOW
g^-

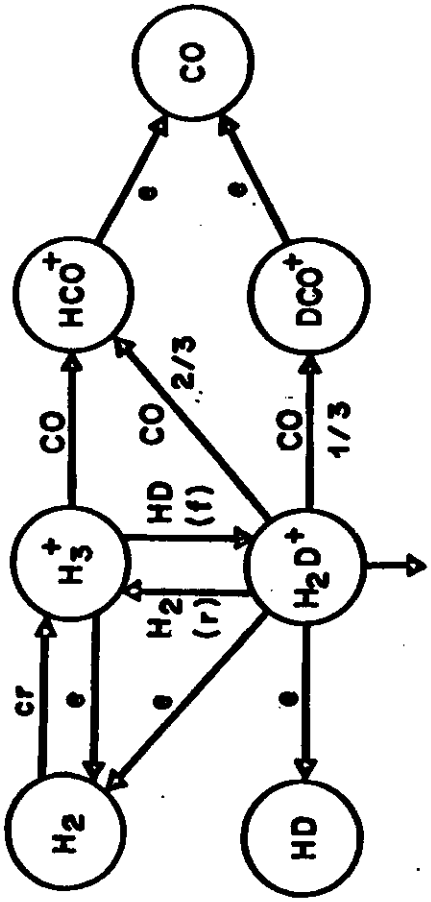
CO
HCO+
DCO+
CO
CO 2/3
CO 1/3
HD (f)
H3+
H2D+
H2 (r)
cr
H2
HD

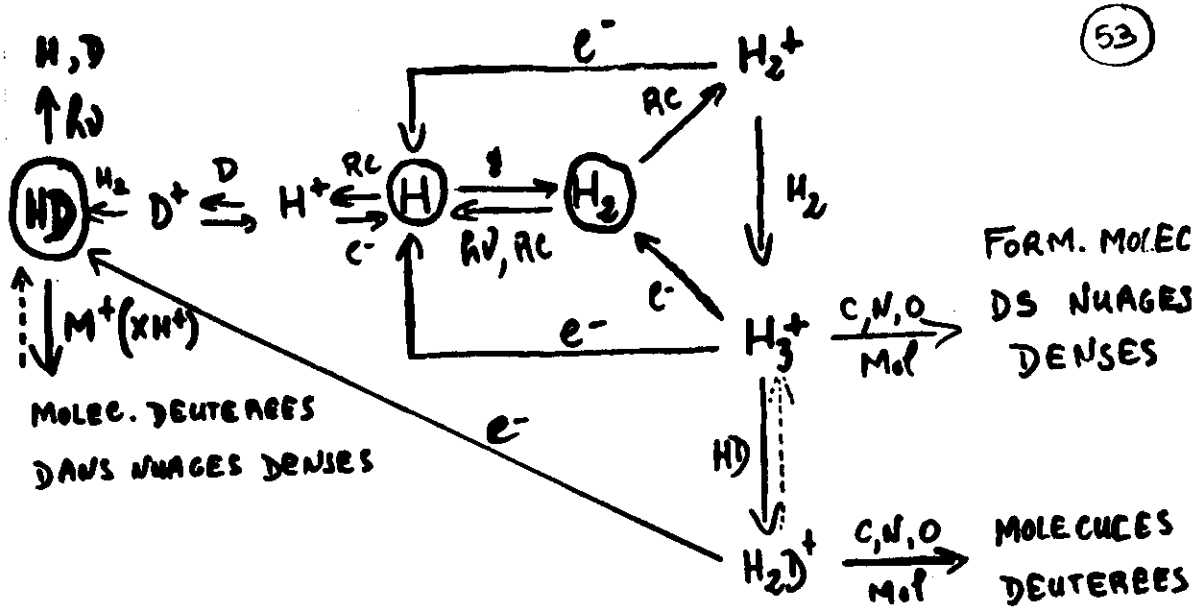
H, D
hν
HD
H2
D+
D
H+
Rc
H
c-
1
H2
hν, Rc
e-
H2+
Rc
H2
e-
H3+
C,N,O
Mol
FORM. MOLEC
DS NUAGES
DENSES
M+(xH2)
MOLEC. DEUTEREES
DANS NUAGES DENSES
e-
HD
H2D+
C,N,O
Mol
MOLECUCES
DEUTEREES
DS NUAGES
DENSES

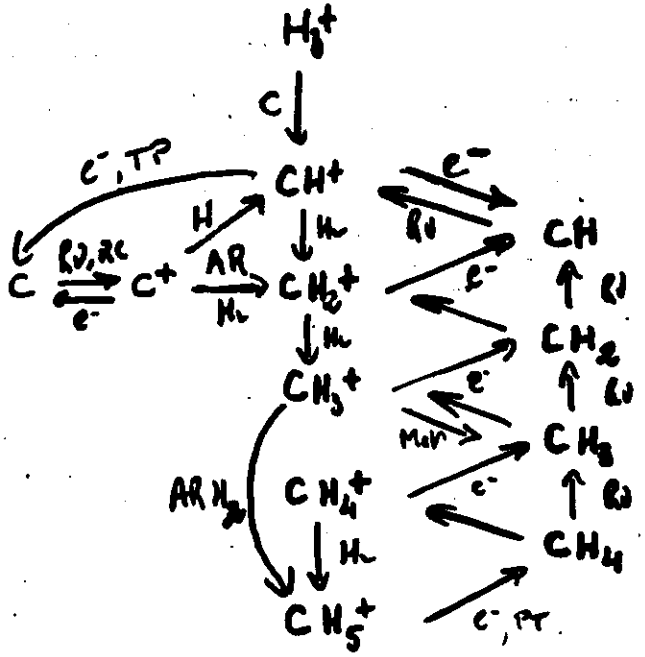

$CH_3^+ + H_2CO \Rightarrow HCO^+ + CH_4 \quad k = 10^{-9}\ cm^3\ s^{-1}$ (mes)

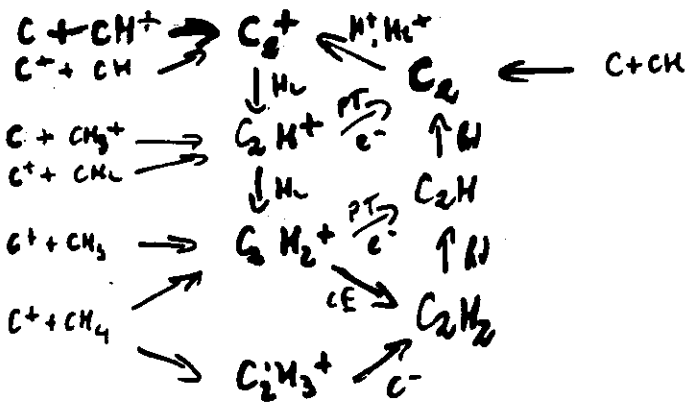

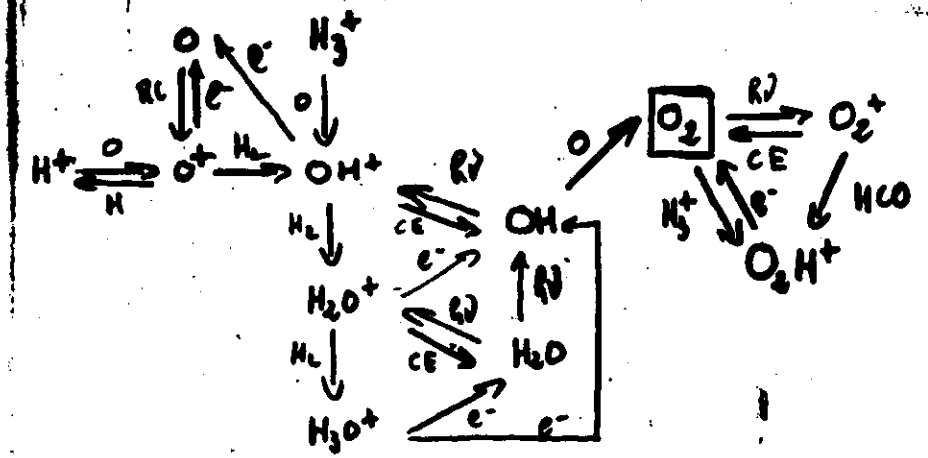

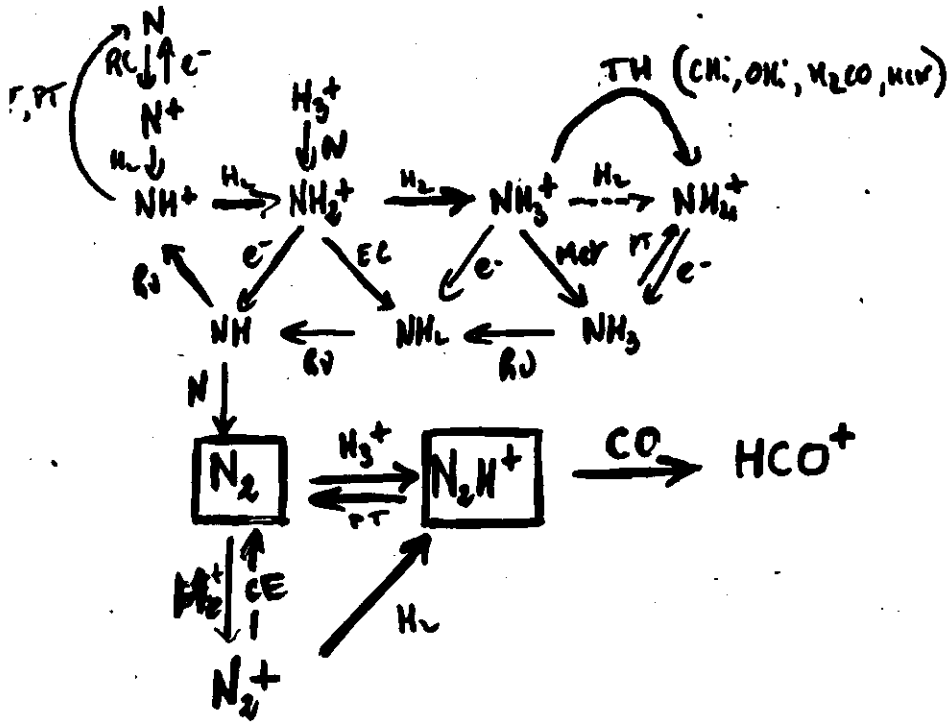

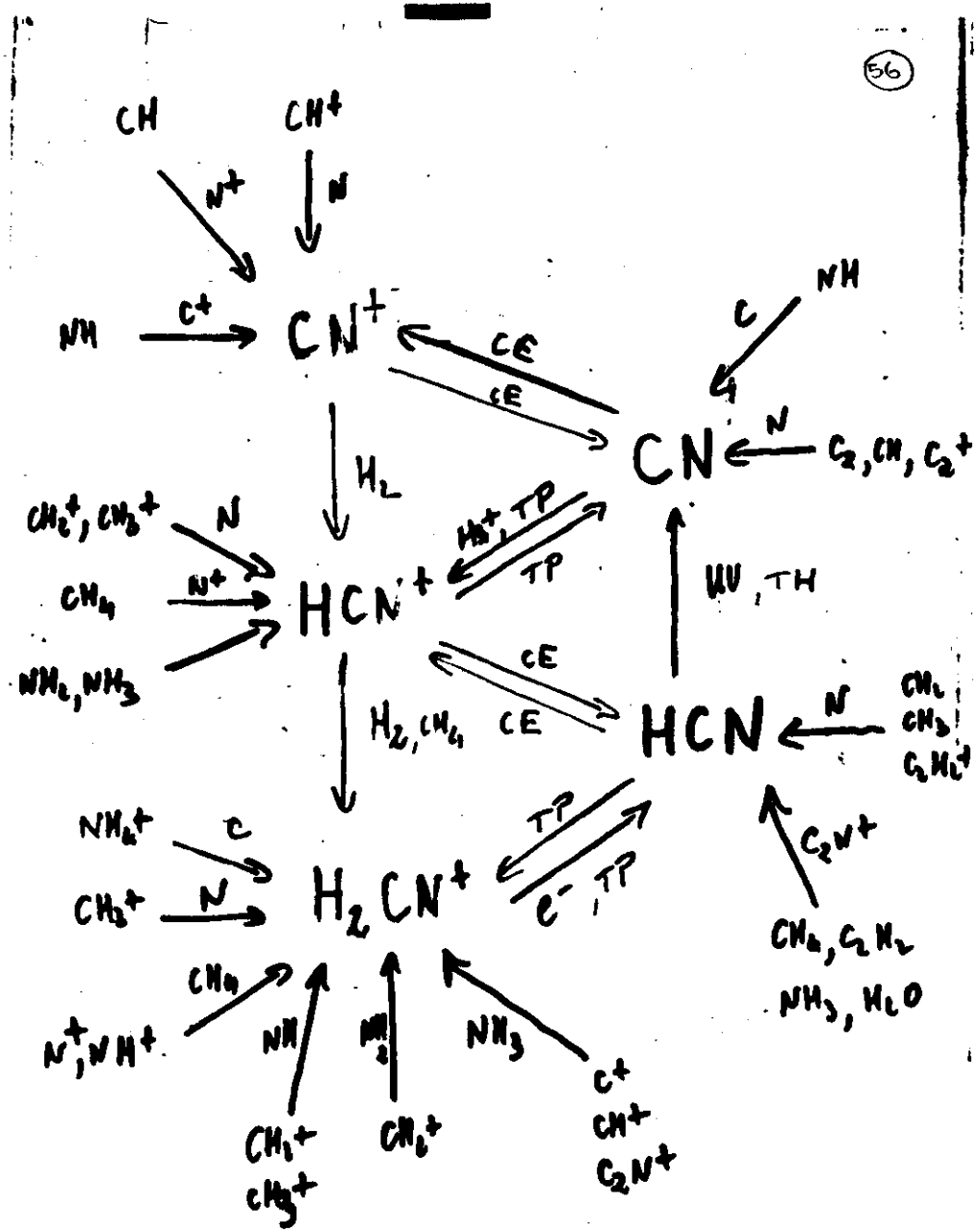

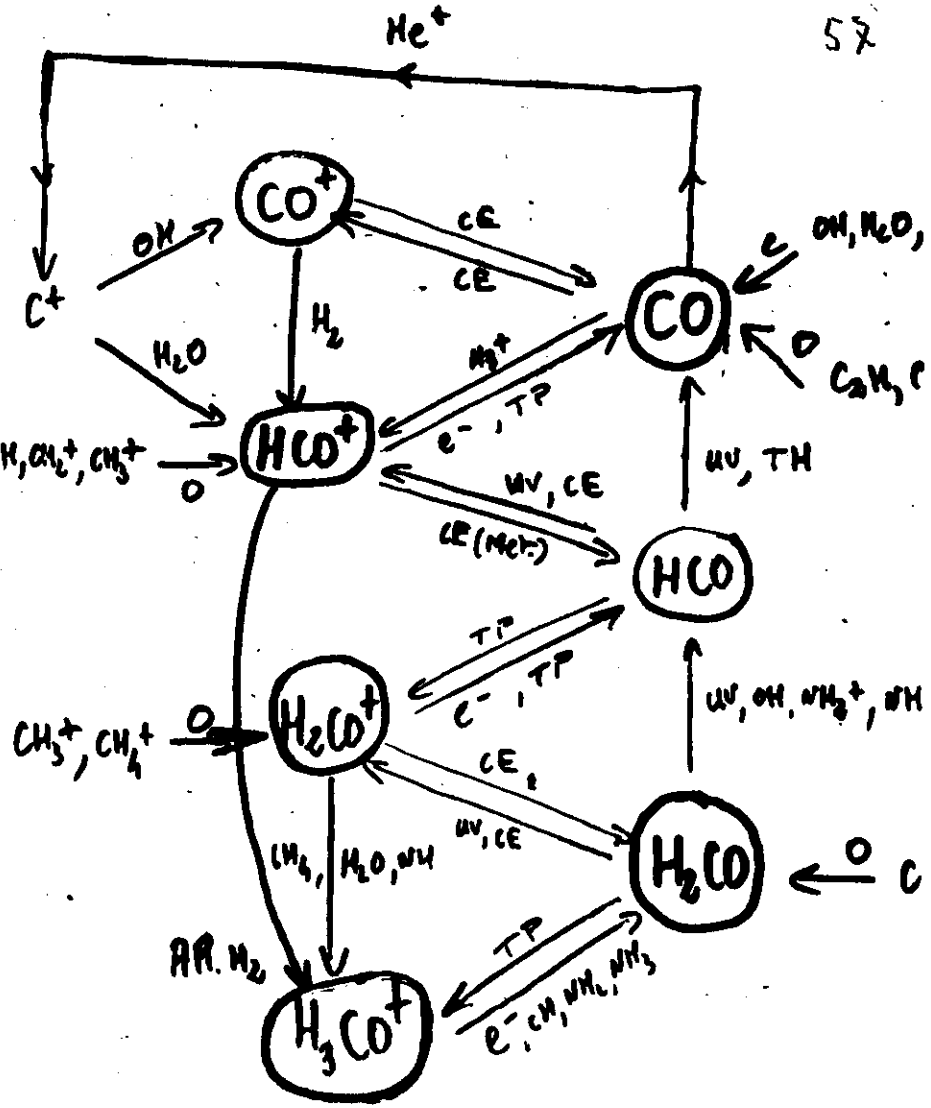

TH : Transfert d'un at. H

CE : échange de charge

TP : Transfert de Proton

UV : Photoionisation - Photodissociation

AR : Arrois radicaux

$$H_3^+ + HD \rightleftharpoons H_2D^+ + H_2 + \Delta E$$

$$H_2D^+ + CO \rightleftharpoons DCO^+ + H_2$$

DCO^+ should be enriched compared to HCO^+, and this is the case (olicle). This chain of reaction is controlled by the local density of electron in the molecular cloud, and permit a precise measurement of the electron density in the cloud.

Watson has also shown that in the case of CO, the exchange reaction

$$CO + {}^{13}C^+ \rightleftharpoons \Delta E + {}^{13}CO + {}^{12}C^+$$

$$\Delta E \sim k \times 40\ K$$

explain the different $CO/{}^{13}CO$ ratio observed in the center of molecular clouds and at the boundaries of such a cloud (in particular for $T_K \simeq 10\ K$).

The recent detection of H_2D^+ (Phillips, 1985), the abundance of DCO^+ clearly indicate that gas phase chemistry is an important tool in the building of complicated molecules. It must be said that there are cases when we do NOT understand how to manufacture molecules: the best cases are CH and H_2CO which seem to be overabundant by 2 or 3 orders of magnitude!

The case of cyanopolyynes ($HC_{11}N$ is observed) is also far from being solved.

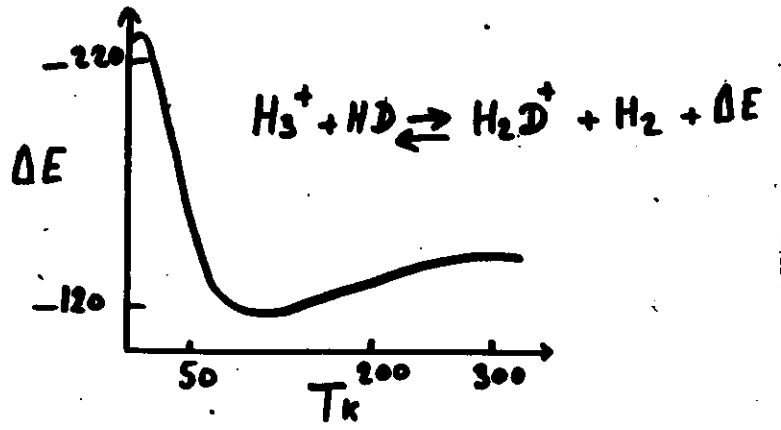

D] A MAJOR DISCOVERY :

The behavior of a small grain (of ~ 50 atoms) being hit by a single U.V. photon led A. Leger and J.L. Puget to suggest that grains of this size would rather be close to coronene ($C_{24}H_{12}$). In comparing their spectroscopic properties, they identified most of the Infrared (2 - 12 μm) unidentified features which had been known for ~15 years. They also predicted that these polyaromatic molecules could emit strongly in the 10 μm band of the IRAS satellite, and this has been recently confirmed (see La Recherche, March 1985).

Their next suggestion is that diffuse bands, which were discovered 70 years ago and which have remained a mystery until today are caused by these molecules. Many groups are presently working on this suggestion, and hope to have the answer in the coming year.

E] A SIMPLE CASE :

The OH radical has been discovered 10 years ago in the gaseous cloud associated with a comet by Gerard and coworkers. On his trajectory, a comet has a velocity relative to the sun which changes with time, and therefore the U.V. excitation of OH can be tested (the Fraunhoffer spectrum of the sun is Doppler shifted). With a single model, it can be shown that period of emission and absorption of Λ doublet of OH should occur at specific velocities, and this has been precisely verified on more than 10 comets (slide).

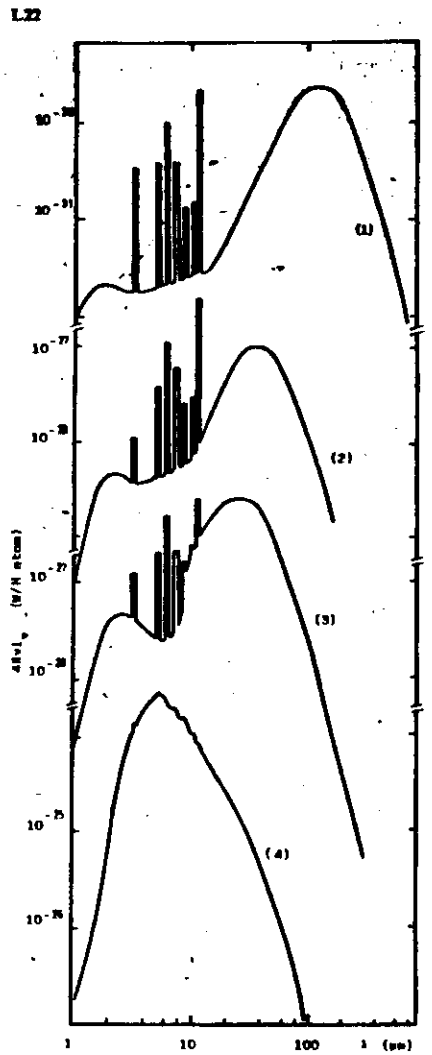

Fig.4 : Spectra obtained for different incident radiation fields : Spectrum 1 : Local Interstellar Radiation Field
Spectrum 2 : 1pc from an 05 star
Spectrum 3 : 0.33 pc from an 05 star
Spectrum 4 : 100 stellar radii from a M0 star

This process should help to measure the rotation period of a comet on itself.

What are the interstellar Molecules used for

A| Star Formation: Physical parameters of molecular clouds

The Molecular Clouds are the places where stars do form after the cloud collapses on itself. It is therefore extremely important to measure the size of the fragments and their density. These objects being opaque to optical radiation can only be investigated with molecular spectroscopy.

The following transparencies show the size of the fragments measured by M. Peault and coworkers using a new technique, and their relation to the thermodynamics of the collapse. 3 sizes seems to fit best with the data.

The electron density n_e, related to the Cosmic Ray flux penetrating these clouds, is measured from the deuterated molecules and their exchange reaction rate. A value $\frac{n_e}{n_{H_2}}$ close to 10^{-8} is deduced by Guélin et al, and explain quite well the ionic chemistry going on.

The magnetic field can be measured directly by Zeeman effect on molecule like OH ($^2\Pi_{3/2}$ ground state). After a decade of painstaking efforts, fields of the order of 11 to 28 μGauss are measured in a few galactic sources. If we recall that from Faraday rotation, the longitudinal magnetic field measured by pulsars is of the order of 3 μGauss, the enhancement in molecular clouds does

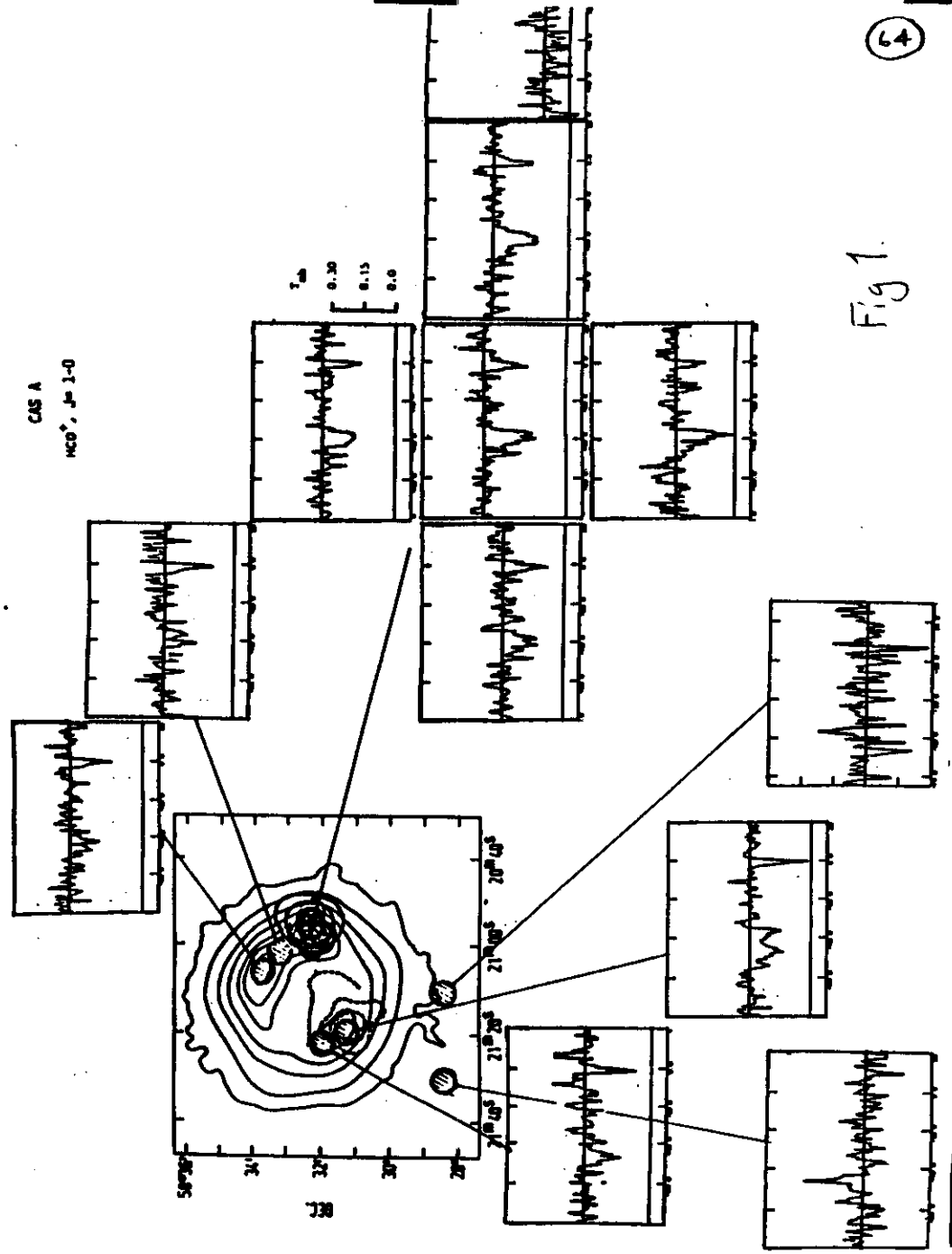

Fig 1

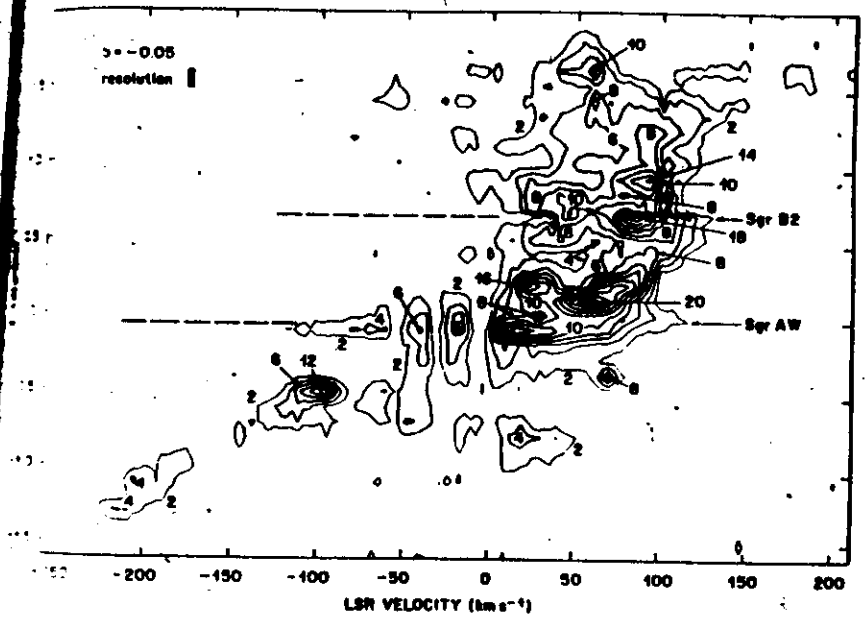

[illegible] at $b = -0^\circ.05$, $l = 2^\circ - 1^\circ.6$. Contours are equally spaced every $\Delta T_A^* = 0.2$ K and are labeled in units of (T_A^* per 0.1 K). Note the [illegible] at −51, −30, −2, and (perhaps) 32 km s^{-1}. The dashed lines at the positions of Sgr B2 and Sgr A W indicate the velocities at which [illegible] from the continuum. Presumably low-excitation HCO^+ is present in the region between these dashed lines and extends to [illegible] galactic longitudes as well.

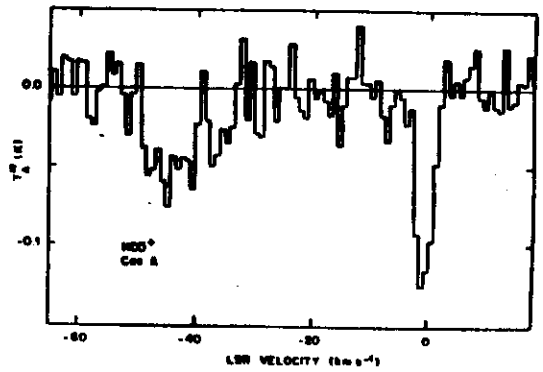

[illegible] absorption spectrum toward Cas A. Continuum emission equivalent to 0.22 K has been subtracted from the baseline. The channels [illegible] km s^{-1} wide. Note that the absorption corresponds to the velocities of the Orion and Perseus arms at 0 km s^{-1} and −45 km s^{-1}.

image classique :

la fragmentation est une conséquence de la contraction

$$M_{Jeans} \propto \frac{T^{3/2}}{n^{1/2}}$$

support uniquement thermique

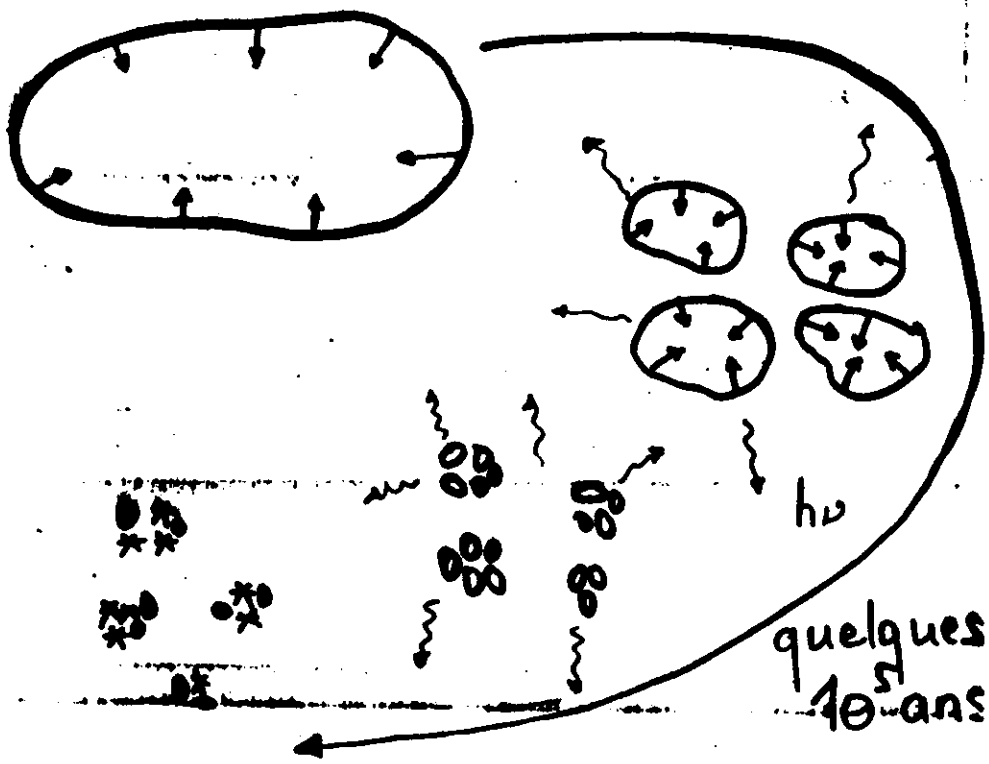

PICTURE OF THE GMC:

- PRIMORDIAL FRAGMENTATION EXISTS BEFORE CONTRACTION
- ASSEMBLY OF ~ 1000 CLOUDS OF 100 $M_\odot$ VIRIALISED IN THE GRAVITATIONAL POTENTIAL OF THE GMC.
- TIME SCALE $>> 10^6$ YEARS
- DENSE CORES HAVE LESS THAN 10% OF THE TOTAL MASS.
- MOST OF THE MASS IS IN THE CLOUDS OF SIZE 1-3 pc
- SCALES ARE SET BY THE EQUATION OF STATE OF ISM ⇒ ONLY $\begin{bmatrix} 1\text{-}3\ pc \\ .1\ pc \end{bmatrix}$ STABLE

IF NO NEIGHBOR: COLLAPSE

HIERARCHICAL STRUCTURE IN MOLECULAR CLOUDS

PERAULT
FALGARONE
PUGET

GMC ~ 10^5 Mo

FRAGMENTS ~ 2 x 100 Mo

DENSE CORES ~ 2-3 Mo

OBSERVATIONS MADE AT BORDEAUX 110-115 GHz
AMHERST 115 GHz
MWO 230 GHz

not follow a single $B \propto n^{1/2}$ law, or it may be that we see only the outer part of the molecular cloud.

By proper star count and a comparison of CO emission, a canonical value $\frac{n_{CO}}{n_{H_2}}$ can be deduced (close to 10^{-4}). A fair amount of carbon is in the form of CO, while the recent detection of the fine structure line of carbon (at submm wavelength) show that an approximately equal amount is in the form of neutral carbon. The remaining part is probably locked on dust grain (or polycyclic molecule).

B] the Galactic Structure:

Surveys of the Galactic plane have been made by different groups using 1 to 10 m class telescope. Of all of them, only part of the sky is fully sampled. The progress in the sensitivity of receivers should permit a complete coverage in the CO 1-0 transition within 2-3 years, while some isotopic survey will be needed later (optical depth effect are not completely understood).

The comparison with HII data show that the galactic structure is well marked in molecular clouds. Except a contrasting limited for years (lifetime of the clouds compared the period of rotation of the Galaxy), it seems now that an agreement has been reached.

The sensitivity of gamma observation is severely limited by the number of photons that the detector sees. It is evident that Giant Molecular Clouds (like the rho ophiuchi complex) are also sources of γ-ray emission (interaction of Cosmic-Rays with the dense molecular gas and π^0-decay).

The comparison with IRAS data is complicated by the fact that part of the emission at 10 μm is due to polyaromatic molecules, while dust is also associated with HI. As can be seen from the enclosed figure, this picture does not agree well with the previous picture of the dust in our Galaxy (as put for the strong infrared-sources).

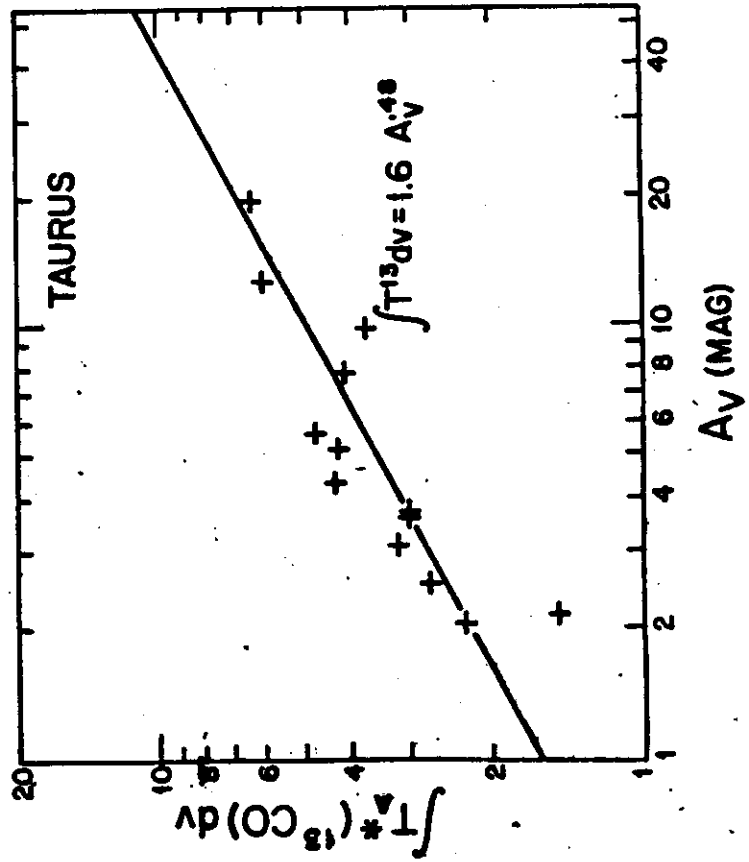

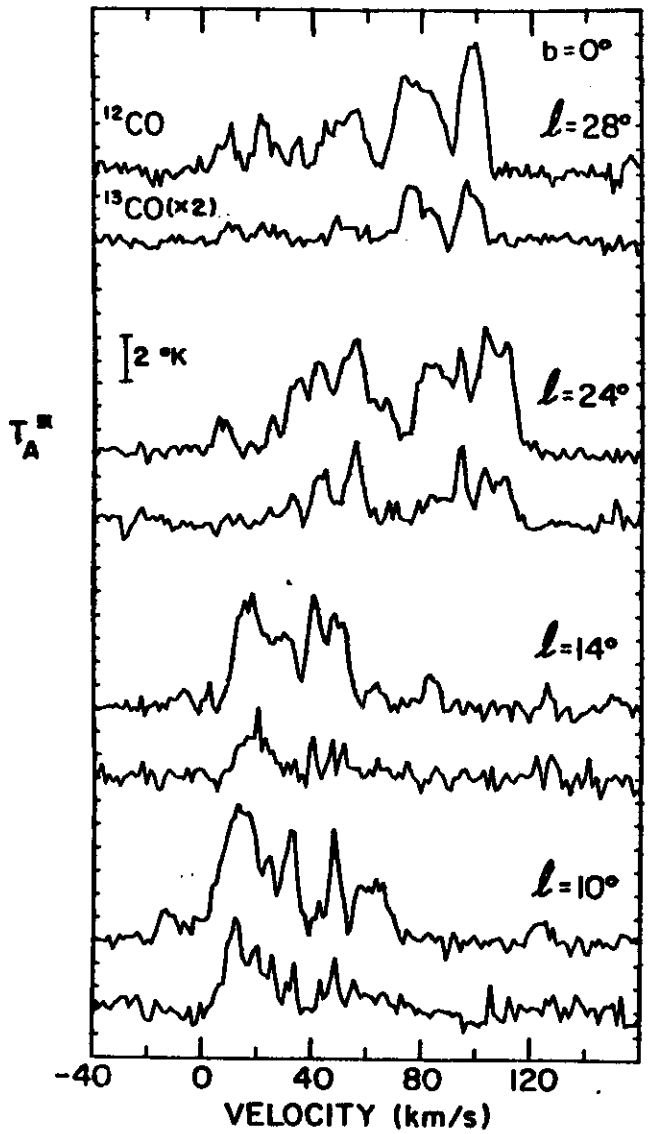

Fig 2. Sample ^{12}CO and ^{13}CO spectra at longitudes 10°, 14°, 24°, 28°. ^{13}CO spectra have been scaled by a factor of 2.

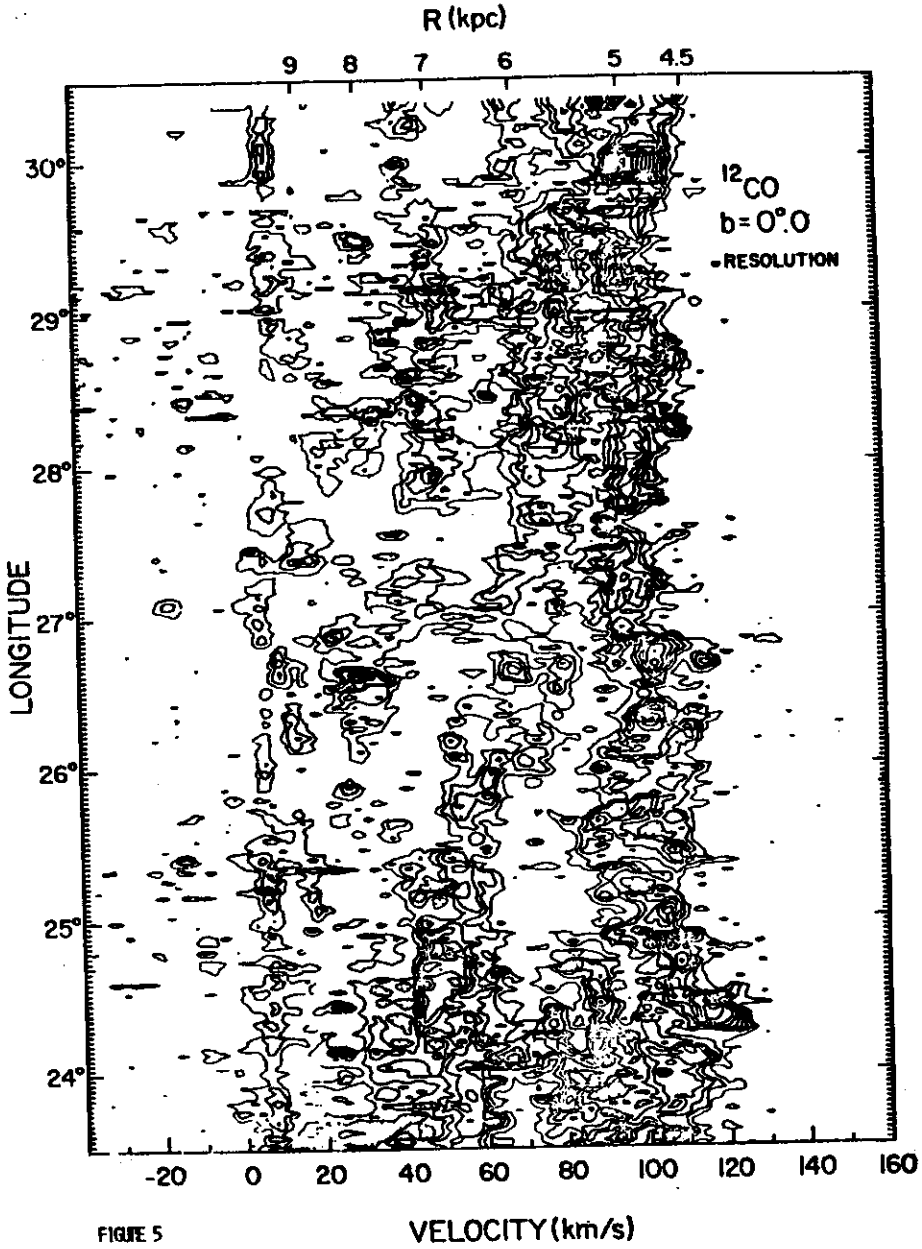

FIGURE 5

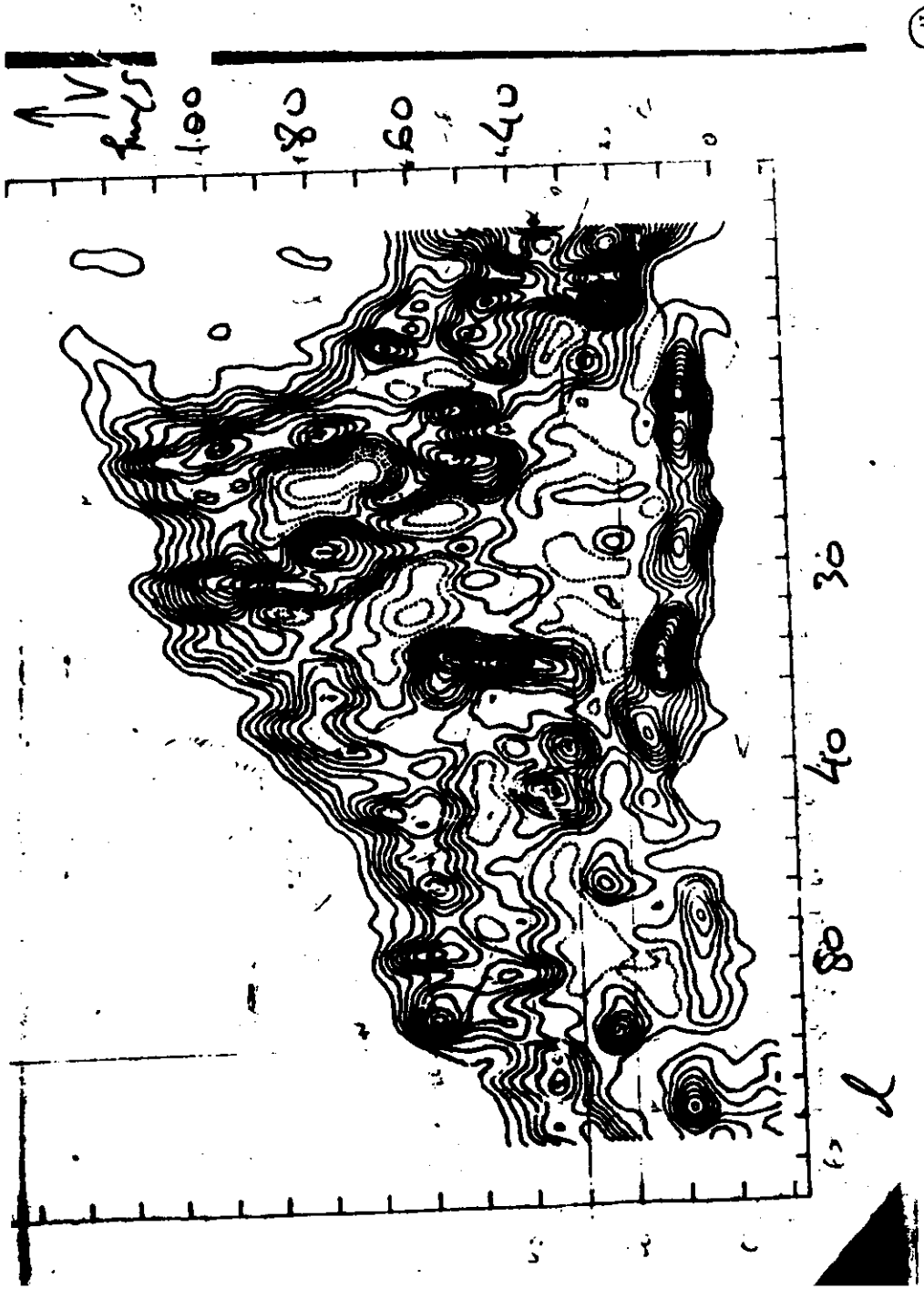
V km/s
-100
-80
-60
-40
30
40
80
l

fig 1 -

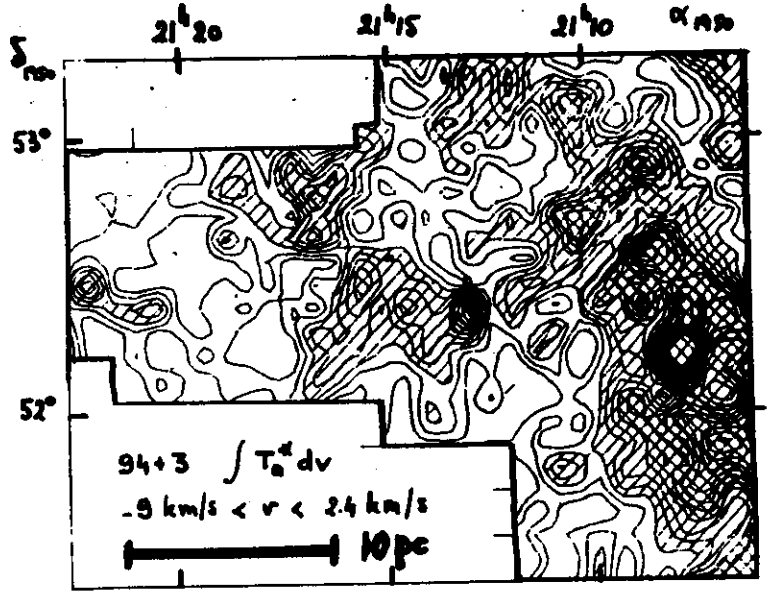
21h20
21h15
21h10
α 1950
δ 1950
53°
52°
94+3 ∫ T_a* dv
-9 km/s < v < 2.4 km/s
10 pc

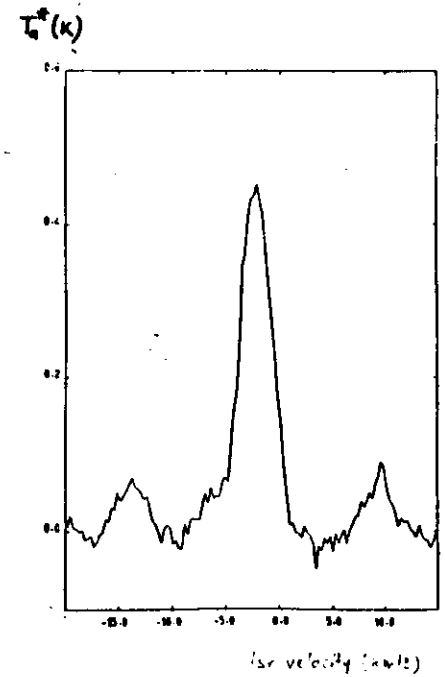
T_a* (K)
(sr velocity (km/s))

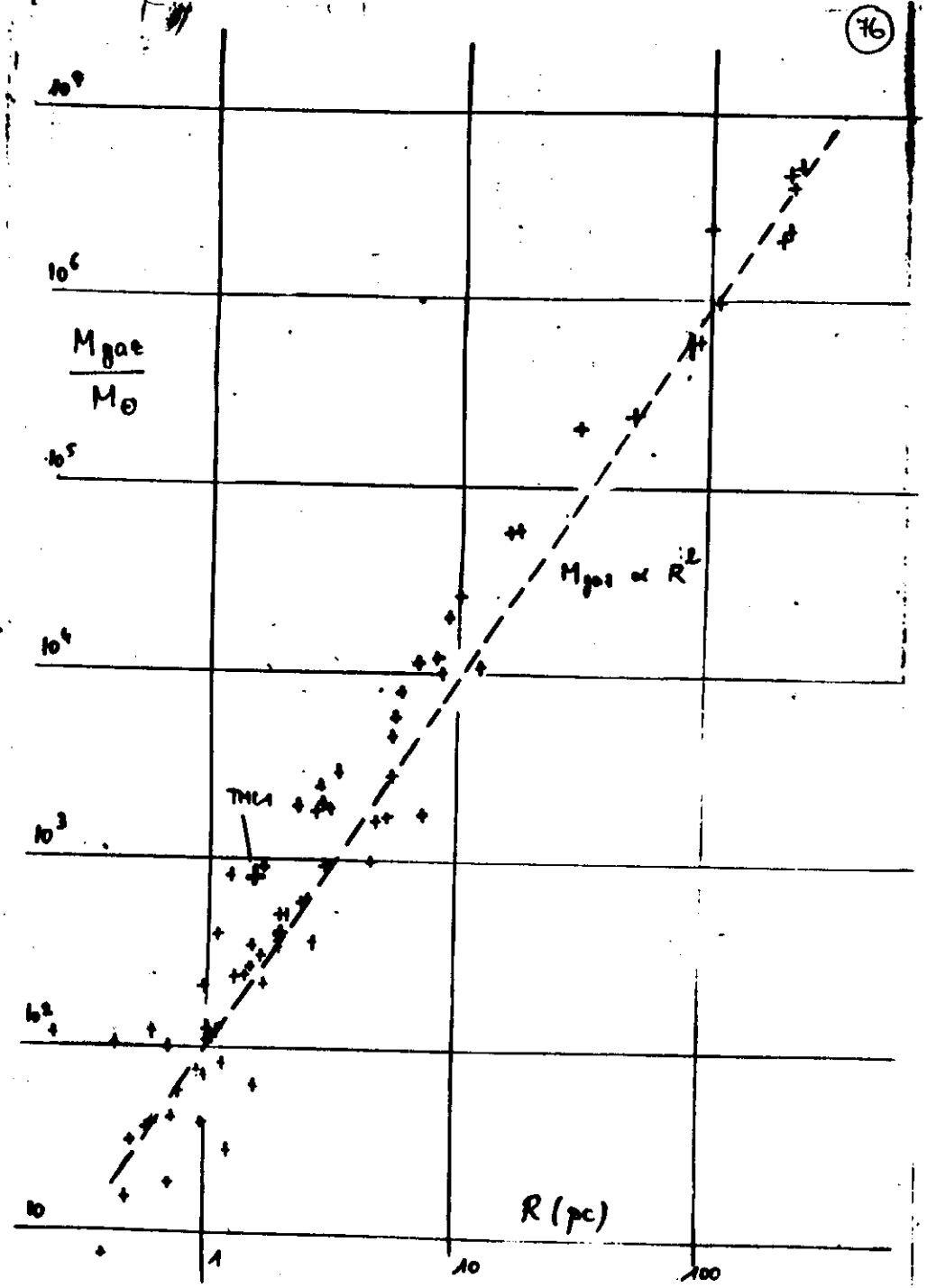
10^9
10^6
$\frac{M_{gal}}{M_\odot}$
10^5
$M_{gal} \propto R^2$
10^4
THEA
10^3
10^2
10
1
10
100
R (pc)

Figure 1

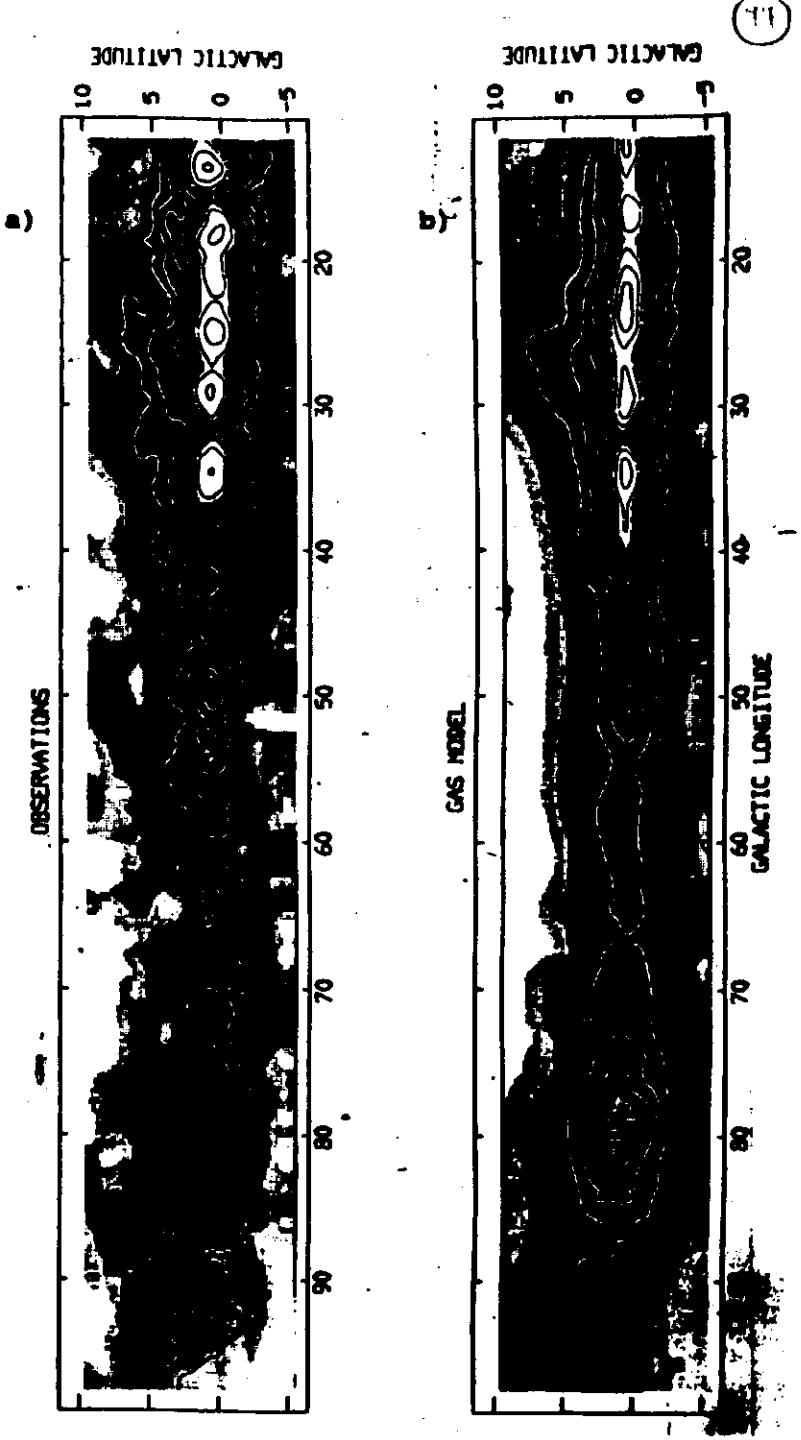
a)
b)
GALACTIC LATITUDE
10
5
0
-5
20
30
40
50
60
70
80
90
OBSERVATIONS
GAS MODEL
GALACTIC LONGITUDE

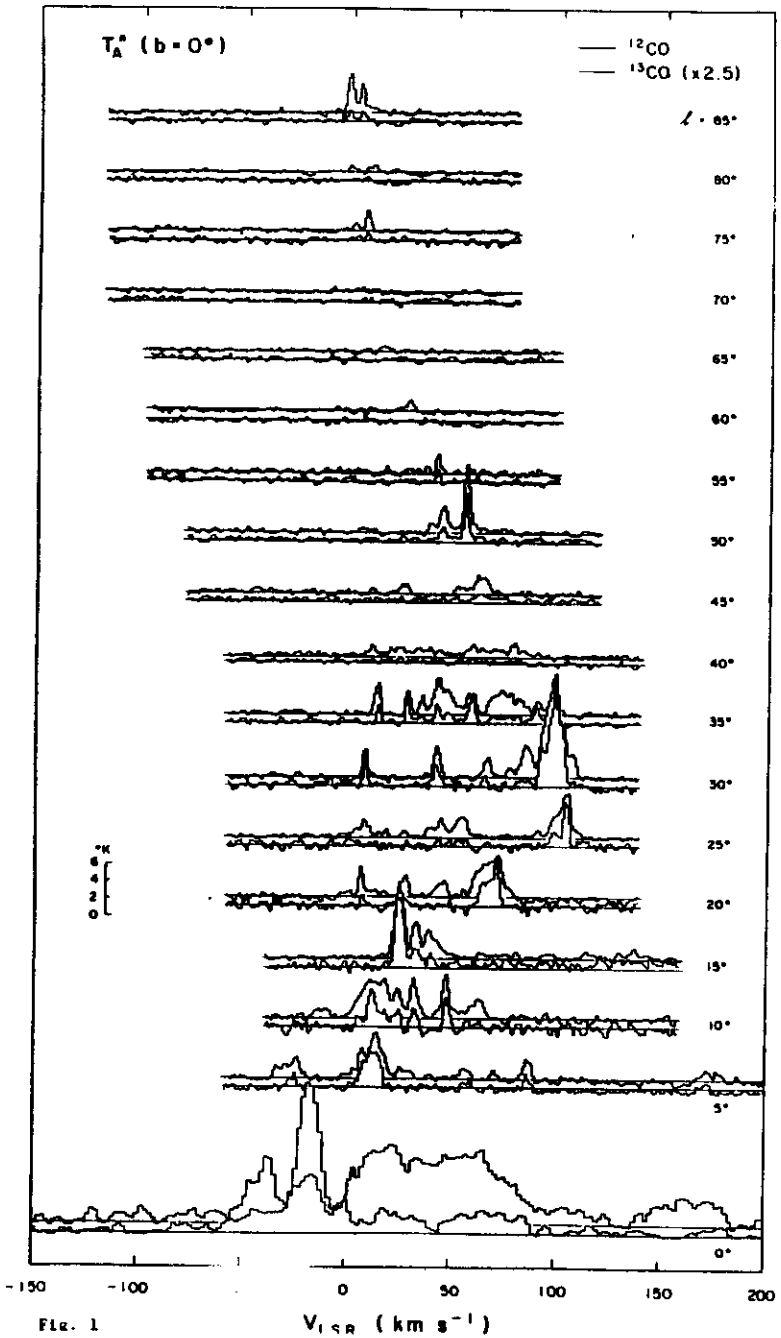
T_A^* (b = 0°)
^{12}CO
^{13}CO (x2.5)
ℓ = 85°
80°
75°
70°
65°
60°
55°
50°
45°
40°
35°
30°
25°
20°
15°
10°
5°
0°
°K
4
2
0
-150
-100
0
50
100
150
200
V_{LSR} (km s^{-1})

Fig. 1

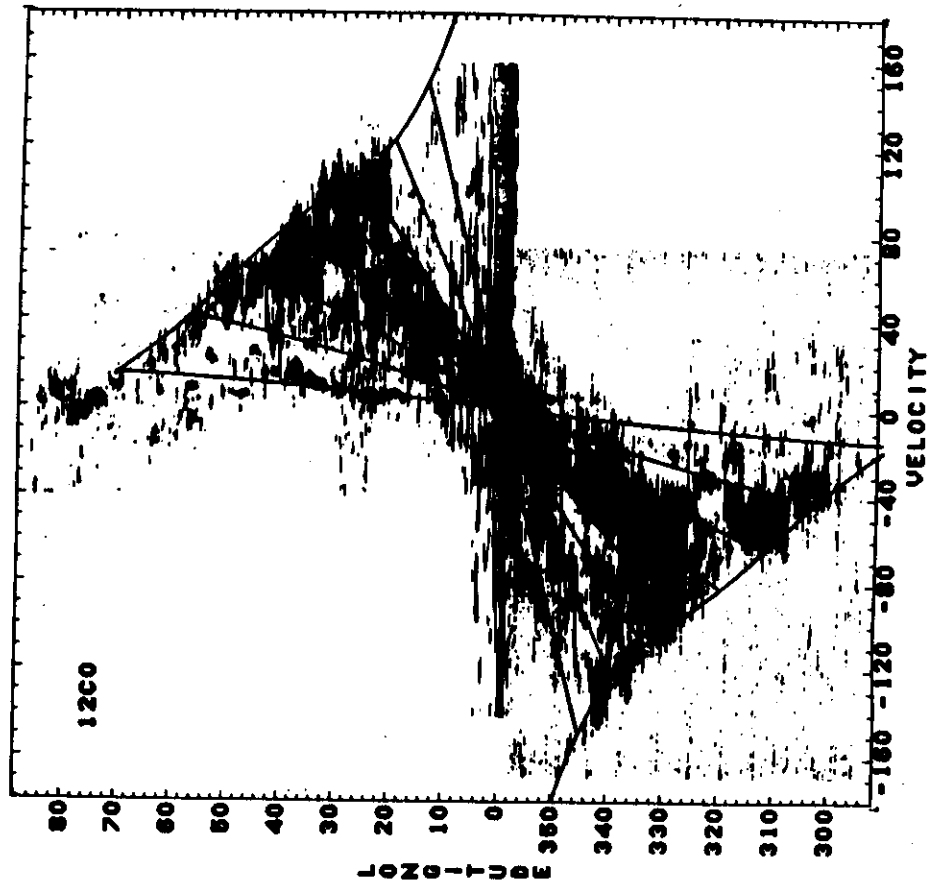
12CO
VELOCITY
160
120
80
40
0
-40
-80
-120
-160
80
70
60
50
40
30
20
10
0
360
340
330
320
310
300
GALACTIC LONGITUDE

Fig. 2

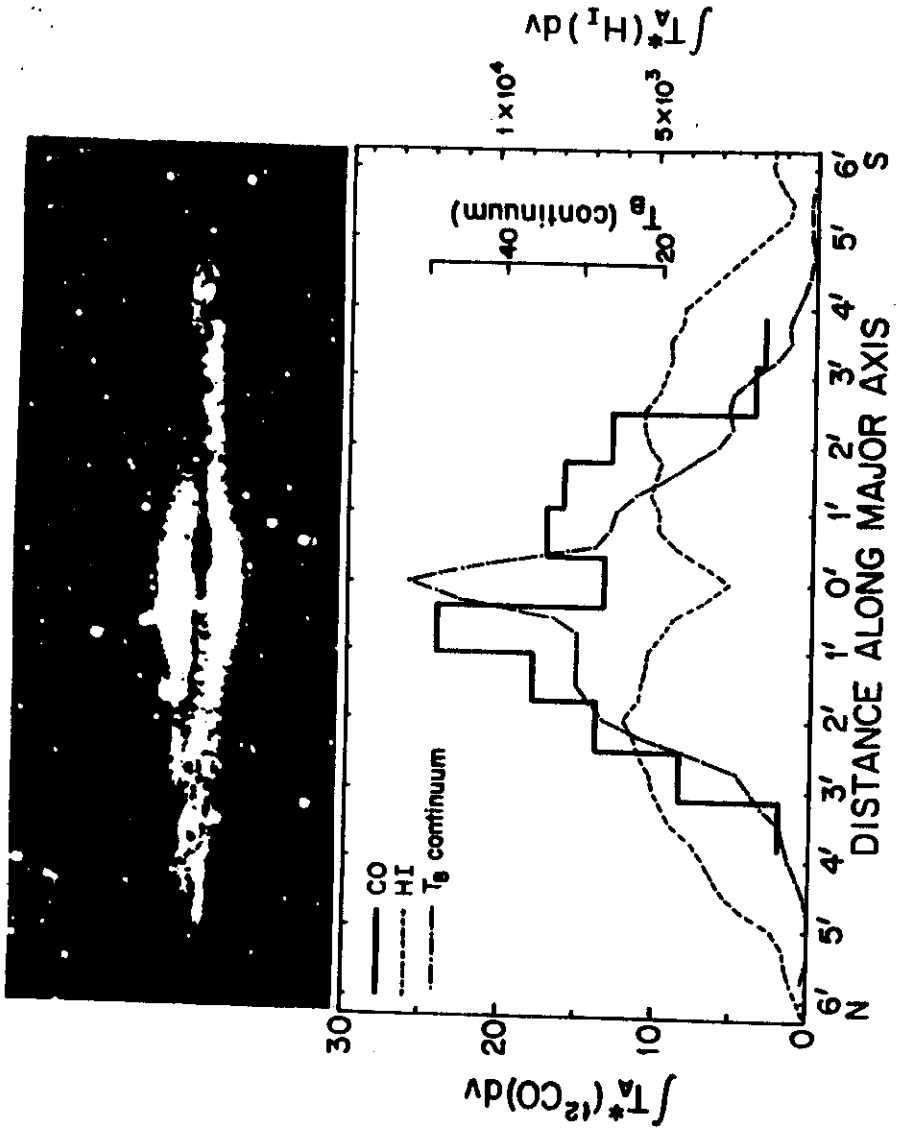

Les poussières interstellaires tissent une véritable toile d'araignée autour du Soleil.

es poussières microscopiques dans le ciel infrarouge ?

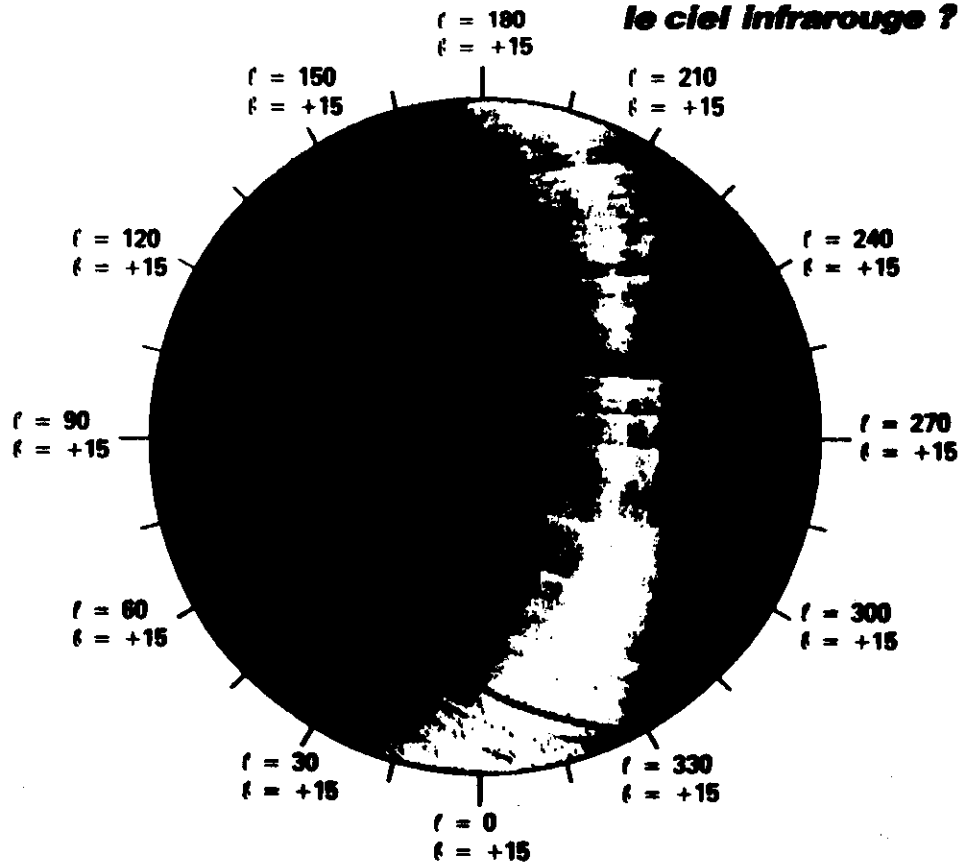

Le 25 janvier 1983 était lancé le premier satellite infrarouge de l'histoire de l'astronomie : IRAS (pour Infrared Astronomical Satellite), fruit d'une collaboration du Royaume-Uni, des Pays-Bas et des États-Unis. Avec son télescope de 57 cm de diamètre, ce satellite permet d'observer le domaine infrarouge dans quatre bandes de longueurs d'onde centrées à 12 μ, 25 μ, 60 μ et 100 μ[1], domaine où les radiations sont complètement absorbées par l'atmosphère terrestre notamment à cause de la vapeur d'eau (le domaine visible s'arrête à environ 1 μ et celui de la radioastronomie commence à 1 mm).

Au bout de dix mois d'observation (il a été arrêté en novembre 1983) IRAS nous a révélé pour la première fois une carte du ciel en infrarouge (voir *la Recherche*, n° 152, p. 254, février 1984). Outre la découverte de systèmes solaires en formation (voir *la Recherche*, n° 150, p. 1596, décembre 1983), IRAS a ouvert la voie à l'étude d'objets et de structures dans l'Univers faits de matière froide et qui n'avaient jamais pu être observés jusque-là[2]. Une de ses découvertes majeures aura sans doute été la mise en évidence de nouveaux constituants de l'Univers : les cirrus infrarouges, des nuages interstellaires constitués de microparticules abondantes en carbone qui tissent une véritable toile d'araignée autour du système solaire.

Un nuage de nuages autour du système solaire

Les nuages de poussières interstellaires peuvent être observés par IRAS car chauffés à de faibles températures, ils émettent principalement de la lumière infrarouge. Tout corps chauffé émet un rayonnement caractéristique de sa température : plus la température est élevée, plus le maximum du rayonnement émis est déplacé vers les longueurs d'onde

(1) G. Neugebauer *et al.*, *Ap. J. Letters*, 278, L1, 1984.
(2) Numéro spécial IRAS, *Ap. J. Letters*, 278, mars 1984.

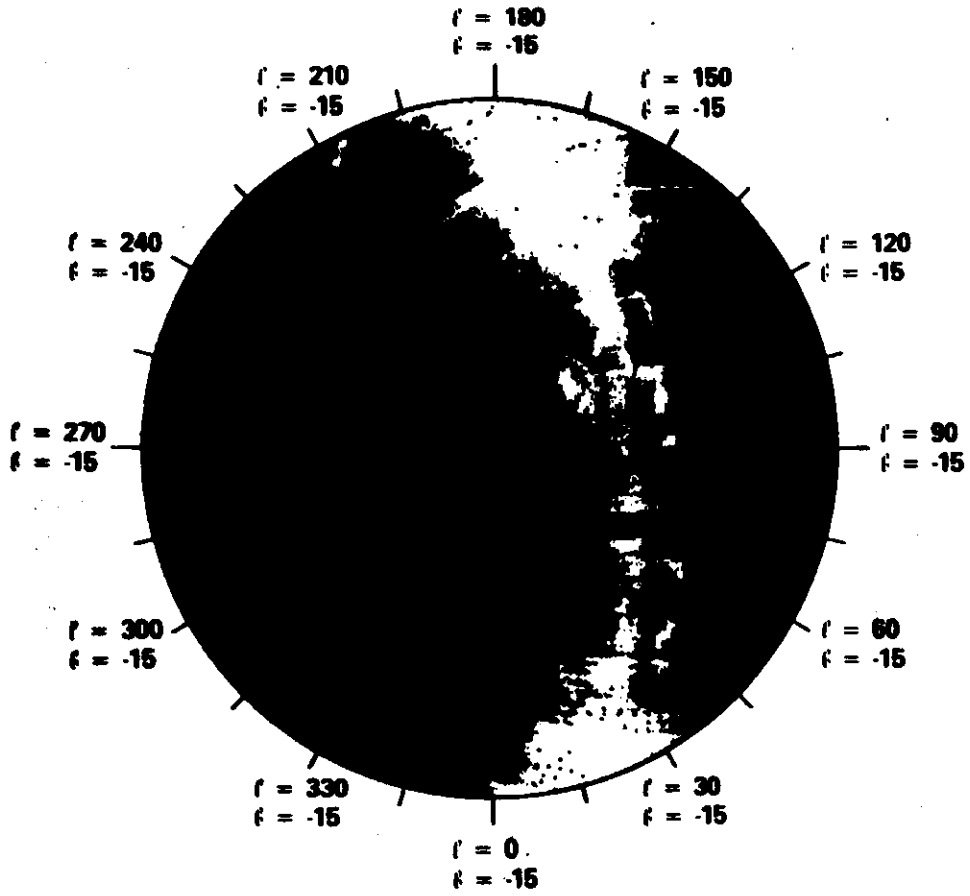

Figure 1. Le satellite d'astronomie infrarouge IRAS a, pendant dix mois en 1983, observé l'ensemble du ciel dans le domaine de longueurs d'onde de 12 à 100 μ : domaine inaccessible aux instruments au sol car totalement filtré par l'atmosphère terrestre. A ces longueurs d'onde, les poussières interstellaires chauffées par le rayonnement ultraviolet des étoiles sont la principale source du rayonnement diffus. Sur ces cartes des deux hémisphères célestes Nord (à gauche) et Sud (à droite) est représentée l'intensité de l'émission telle qu'elle a été observée par IRAS (les zones les plus intenses apparaissent en jaune et rouge, les plus faibles en bleu et noir). Chaque carte est centrée sur chacun des pôles Nord et Sud de la Galaxie et graduée en longitude (ℓ) et latitude (ß) galactique. La bande sombre et étroite (de l = 90° à l = 270°) correspond à des régions qui n'ont pu être observées. A l'exception des nébuleuses d'Orion et de la Carène qui apparaissent comme deux taches brillantes (vers l = 210° et l = 265°), le reste de l'émission est remarquablement uniforme.
A la grande surprise des chercheurs, les nuages de poussières qui apparaissent ainsi ne sont ne correspondent pas aux concentrations de matière interstellaire connues jusque-là. Ils se répartissent uniformément, couvrent le ciel infrarouge de structures filamenteuses : des cirrus infrarouges d'aspect analogue aux cirrus de l'atmosphère terrestre. Ces nouveaux composants de l'Univers sont encore très énigmatiques. Les caractéristiques de leur émission infrarouge suggèrent une composition de micrograins à forte teneur de carbone qui pourraient être en fait un agrégat de grosses molécules cycliques. Leur origine reste encore mystérieuse et leur distance exacte est encore inconnue. (Cliché JPL).

courtes, la relation entre les deux étant donnée approximativement par T = 2 900/λ où λ est la longueur d'onde en microns et T la température en degrés Kelvin. Dans le domaine couvert par IRAS (12 à 100 μ) émettront donc essentiellement des corps chauffés à des températures de 30 à 250 K (soit - 243 à - 23 de nos degrés Celsius).

Or on a pu calculer que, dans la Galaxie, les différents types de rayonnements présents (rayonnement ultraviolet des étoiles, particules de haute énergie du rayonnement cosmique...) étaient suffisants pour chauffer les poussières interstellaires à des températures de l'ordre de 25 à 30 K. Un unique type de poussières était connu jusque-là : des grains de silicate d'une taille de 0,01 à 1 micron mélangés au gaz de la Galaxie et distribués approximativement comme lui, c'est-à-dire concentrés dans le plan galactique. La cartographie du ciel établie par IRAS à la longueur d'onde de 100 μ aurait donc dû révéler ces poussières approximativement selon le dessin de la Galaxie.

Or, à la grande surprise des chercheurs, l'émission observée à cette longueur d'onde n'est pas particulièrement localisée, mais semble venir de toutes les directions (fig. 1). Elle couvre l'ensemble du ciel infrarouge de structures filamenteuses à la manière de certains nuages terrestres qui sont les cirrus, ce qui leur a valu d'être baptisés « cirrus infrarouges ».

A cause de l'uniformité de leur répartition, ces cirrus correspondent sans doute à de la matière interstellaire proche qui, comme un cocon, entoure le système solaire. Il est impossible à l'heure actuelle de fixer plus précisément leur distance. Il a été suggéré qu'une partie de ces nuages soit en fait très proche et située aux confins du système solaire (à une distance inférieure à une année-lumière), mais la majorité est sans doute interstellaire à des distances approximatives de 600 années-lumière.

Dans l'étude de ces cirrus infrarouges, une deuxième surprise allait venir des cartes établies par IRAS aux trois autres longueurs d'onde. Ces nuages apparaissent en effet de façon très claire sur la carte à 60 μ, et F. Boulanger de l'Observatoire de Meudon, actuellement à l'université de Groningen, a découvert qu'ils émettaient également un rayonnement à 12 et 25 μ ! L'émission à ces longueurs d'onde, bien que quatre fois plus faible que celle à 100 μ, est beaucoup plus importante que celle que l'on pouvait envisager pour la poussière interstellaire.

Où la poussière abonde
hors des étoiles.

Cette émission était d'abord passée inaperçue à cause de la lumière zodiacale, due aux poussières qui existent également à l'intérieur de notre système solaire. Du fait de l'attraction du Soleil, ces pous-

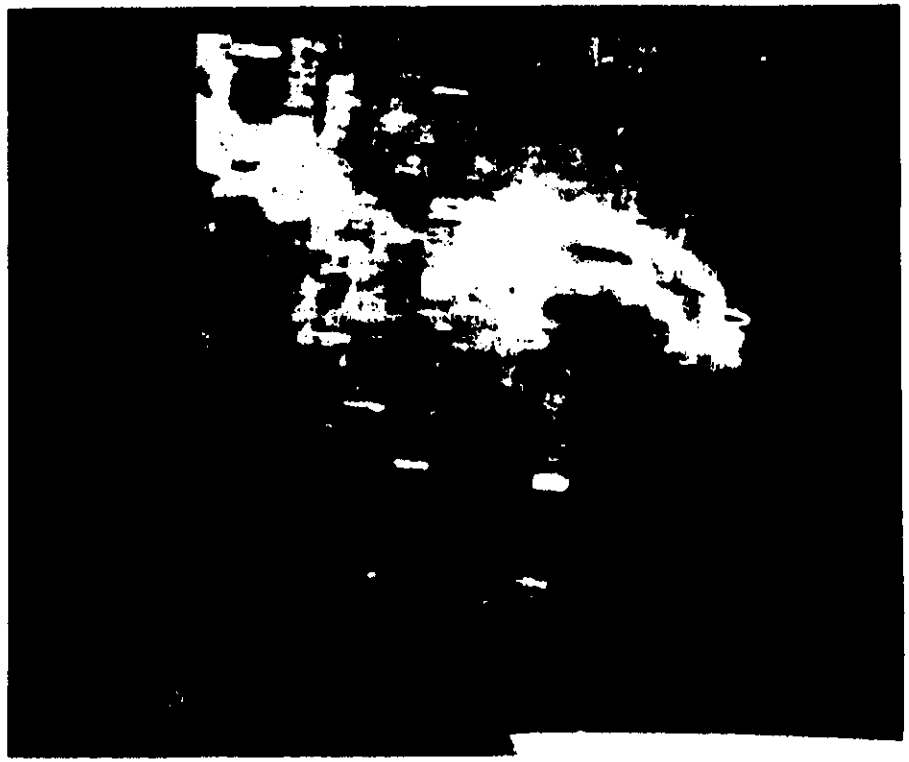

Figure 2. Les sources brillantes de rayonnement infrarouge sont les poussières interstellaires chauffées par le rayonnement ultraviolet des étoiles. Dans la Galaxie, les nuages moléculaires (des nuages où la densité du gaz d'hydrogène interstellaire est suffisante pour recombiner l'hydrogène atomique en molécules H_2) contiennent une forte proportion de poussières. Sur cette photo prise par IRAS à la longueur d'onde de 12 μ, dans une région du ciel de 3°5 par 3°5, le nuage moléculaire B Carène Australe apparaît clairement. L'intensité du rayonnement infrarouge émis est représentée par une échelle de couleurs (indiquée au bas de la figure). Le rayonnement infrarouge observé par IRAS pour plusieurs de ces nuages est trop élevé pour être émis par des poussières de taille « normale » (0,01 à 1 micron) chauffées par le rayonnement galactique ambiant. Il pourrait, en revanche, s'expliquer si une certaine proportion de la poussière dans ces nuages moléculaires était de même type que celle suggérée par les cirrus infrarouges, c'est-à-dire des micro-grains de quelque 0,0005 micron de diamètre. (Cliché A. Leene et P. Wesselius.)

C/ Extragalactic Molecular Astronomy: a field in its infancy

Since its discovery in 1975, 200 galaxies have been observed and approximately 60 detected. The main problems associated with these observations are the lack of sensitivity
lack of resolution

The main beam is:

BTL	1.7'
KPNO	1'
UMASS	50"
Sweden	33"
IRAM 30m	22"
Nobeyama 45m	15"
Cal Tech 3x10m	8"

Selection effects are strongly affecting the data:
- inclination of the galaxies
- dilution in velocity

The advent of more sensitive receivers and larger collecting areas should suppress this bias.

The main results can be summarized as follows:
- radial distribution of CO/HI
- n(He)/n(HI)
- Spiral structure } only in M31
- Size of the Giant Molecular Clouds }

Isotopically substituted molecules have been observed for the first time in M31 (^{13}CO) and in M82 ($C^{18}O$). The ratio to the main line is difficult to analyze.

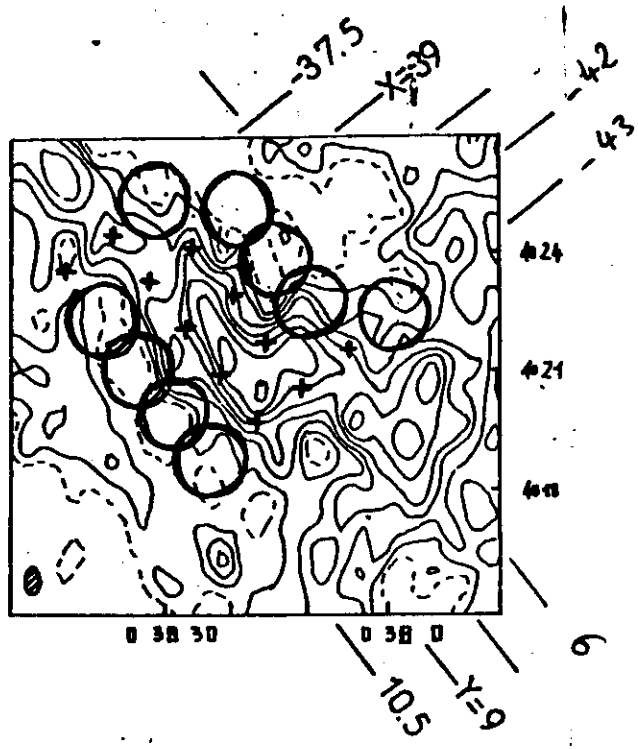

M31

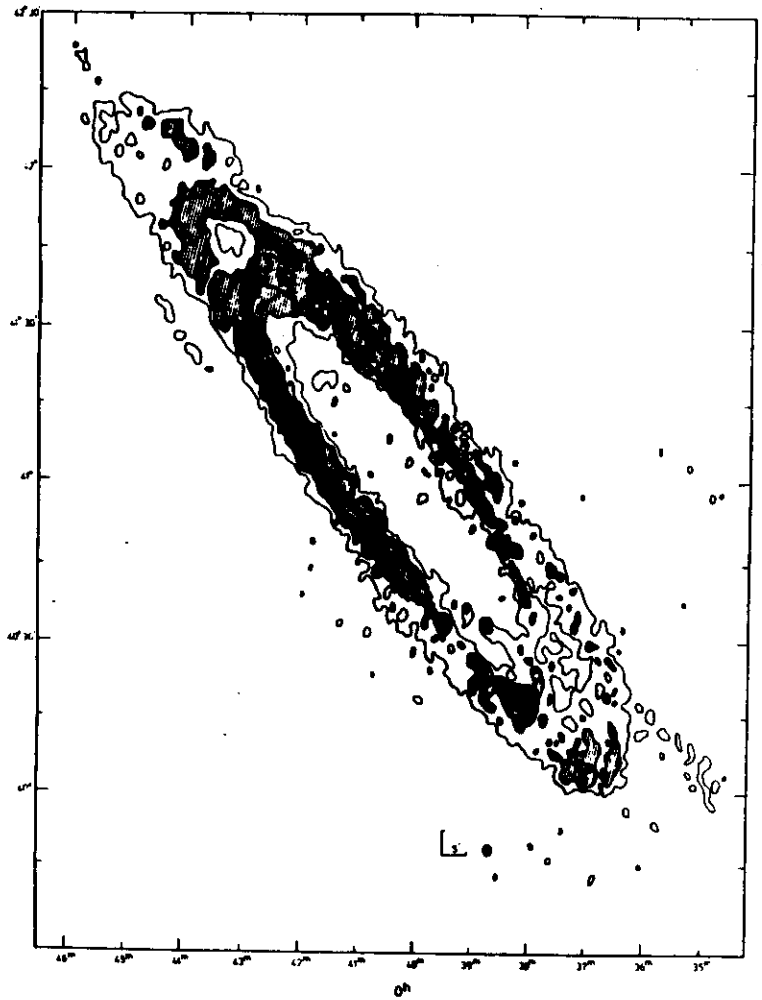

FIG. 1. Integrated HI emission from M31. The beam size of 1.5 x 2.2 arc min is shown as a shaded ellipse. The contour interval is 600 K km s^{-1}, with regions above the 1200 K km s^{-1} level, and also the 2400 K km s^{-1} level, being shown shaded. The so-called "SW companion" of M31 is not shown, being beyond the SW extension of this map.

(86)

(87)

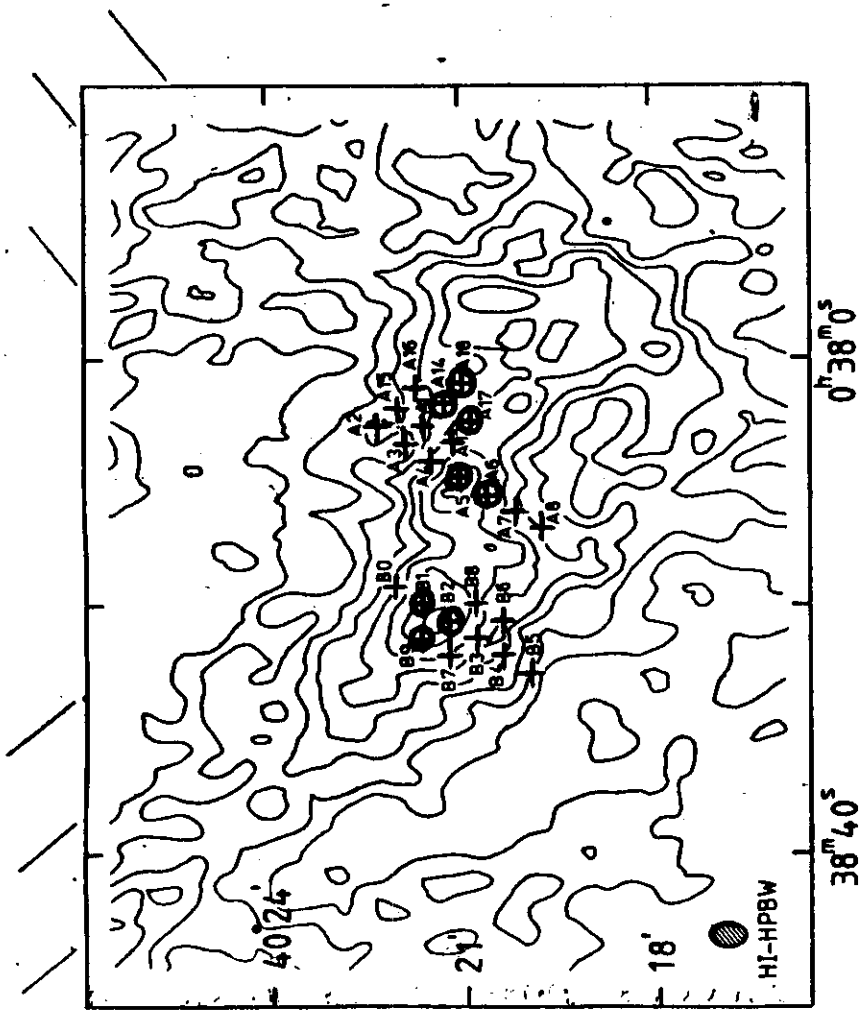

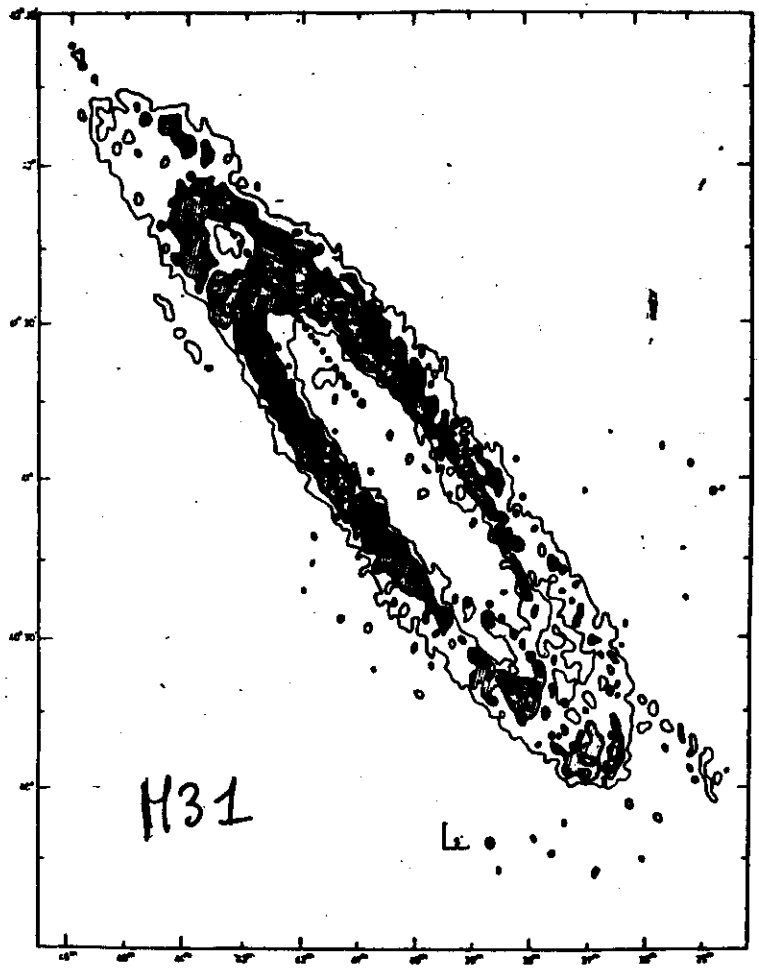

Lilt Peak (78)

Galaxies cartographiées en CO

	Type	Anneaux	i	Nbre de lobes	D Mpc
M31	Sb	⊗	77	24000	.7
N253	Sc AB		79	160	2.5
M33	Scd	points	55	3100	.7
N891	Sb	?	88	9	9.5
N1068	Sb		43	50	16
N2403	Scd AB	points	60	230	3.2
N2841	Sb	⊗	68	36	9
N2903	Sbc AB	3 points	70	45	6
M82	Irr	filaments	66	43	3.2
N3627	Sb AB		60	55	9
N3628	Sb pec		76	77	9
N4254	Sc		27	9	20
N4258	Sbc AB		72	50	5
N4321	Sbc AB		35	55	20
M51	Sbc		20	71	7.6
M83	Sc AB		24	100	4.3
N5248	Sbc AB	⊗	55	20	15
M101	Scd AB		22	590	5.5
N6946	Scd AB		30	90	4.6
N7331	Sbc	⊗	75	43	15
IC342	Scd AB		25	415	3
Maffei 2	Sb		60	43	4

NGC 5236 (M83)
from Combes et al (1978)

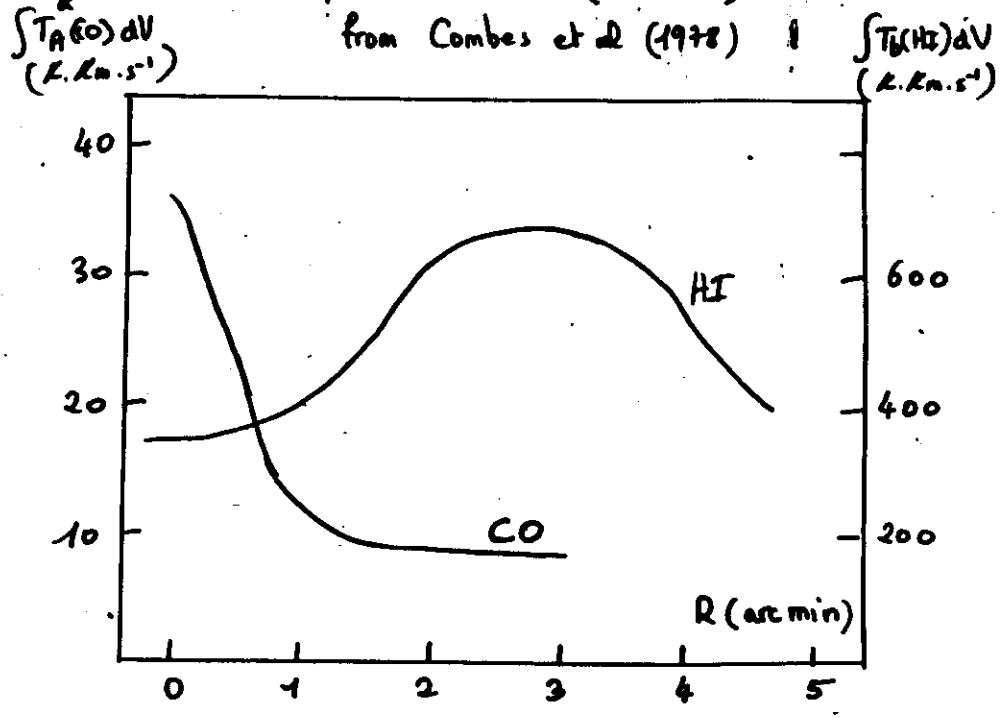

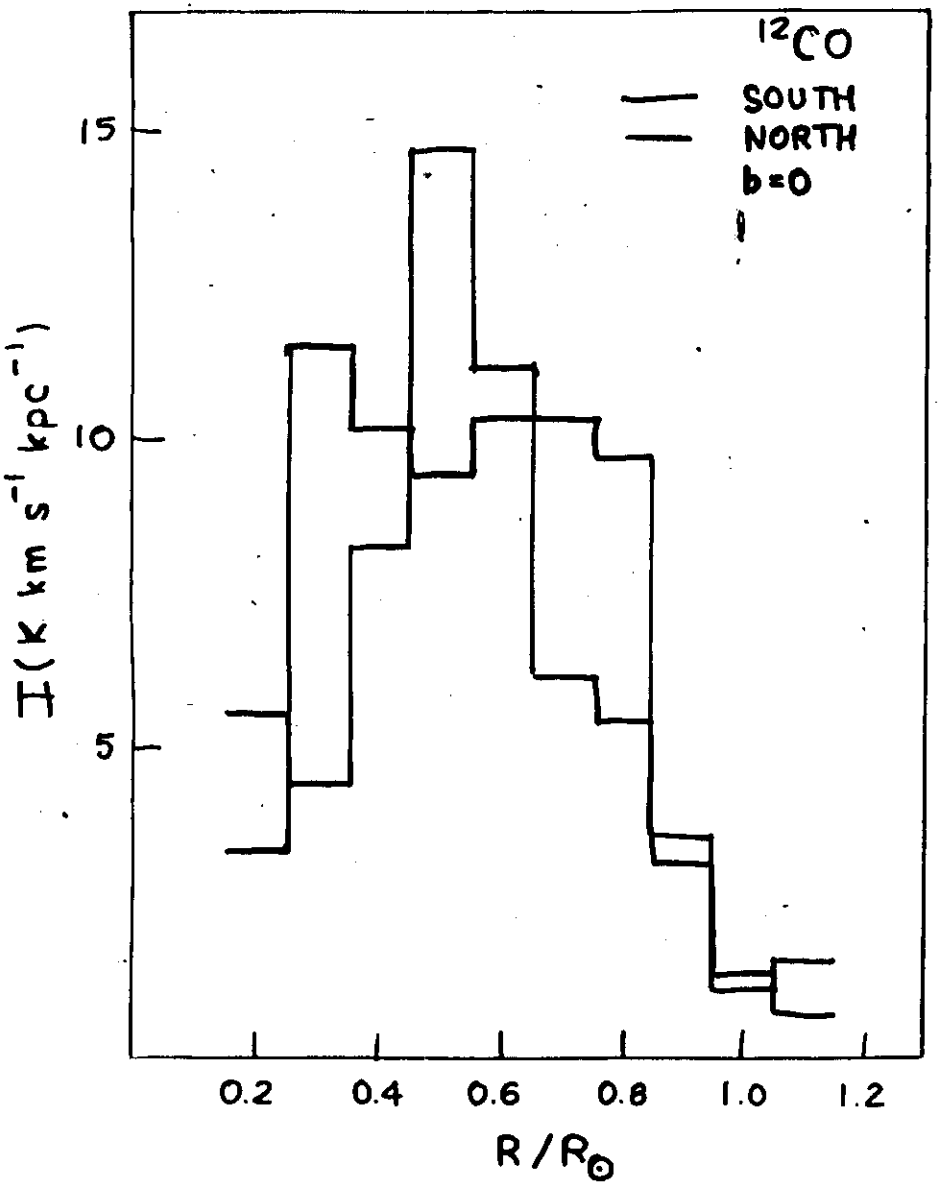

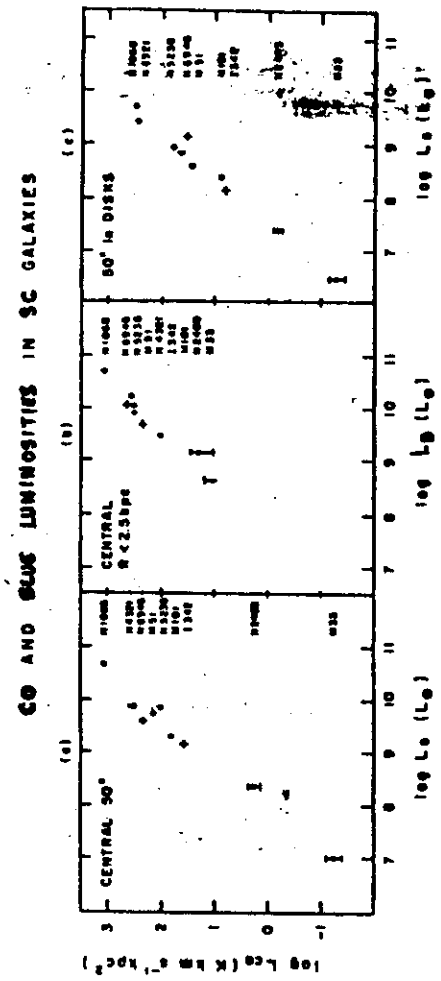

Figure 7. Comparison of CO and blue luminosities in (a) the central 50", (b) regions 5 kpc in diameter centered on the nuclei, and (c) regions 50" in diameter in the disks for nine galaxies (L_{CO} ≡ I_{CO} x Area Beam). Over four orders of magnitude in luminosity, a linear correlation is evident. The open circle represents the Seyfert galaxy NGC 1068 which has the highest luminosity. The uncertainties in L_{CO} are given for M33 and NGC 2403, and for the other galaxies are smaller than the dots plotted. Distance uncertainties do not alter the correlation since both luminosities depend on D^2. The best fit to the data in (b) is $L_B = 4 \times 10^7 L_{CO}^{1.0}$.

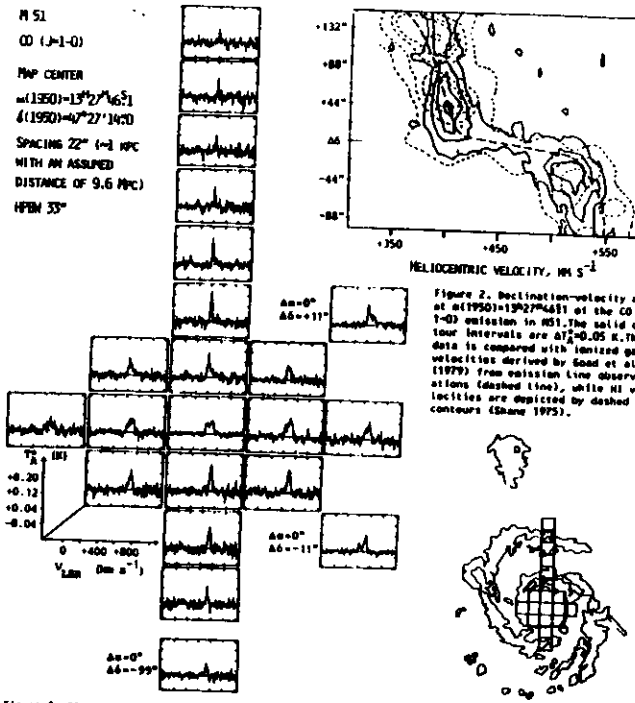

Figure 2. Declination-velocity map at α(1950)=13h27m46.6s of the CO (J=1-0) emission in M51. The solid contour intervals are $\Delta T_A^* = 0.05$ K. The data is compared with ionized gas velocities derived by Goad et al. (1979) from emission line observations (dashed line), while HI velocities are depicted by dashed contours (Shane 1975).

Figure 1. CO emission in M51. The inset diagram shows the position of the spectra on a tracing of the optical outline of the galaxy. The intensity scale is given in antenna temperature corrected for radome and atmospheric attenuation. The main beam efficiency is 0.5 and the moon efficiency is 0.6. To get from V_{LSR} to heliocentric velocity, subtract 11.7 km s^{-1}.

(94)

(95)

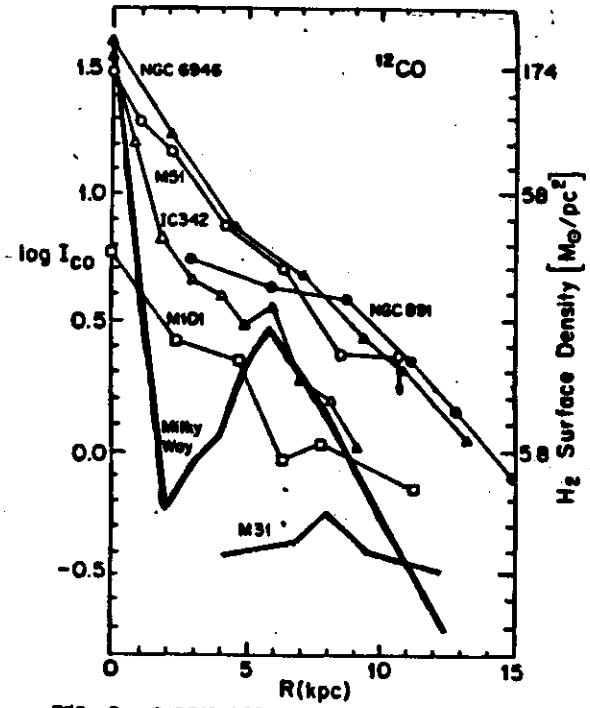

FIG. 9. RADIAL DISTRIBUTION OF CO EMISSION IN 6 GALAXIES COMPARED WITH THE MILKY WAY.

MILLIMETER RADIO TELESCOPES:

		ϕ(m)	λ_{min}
SINGLE DISH:	EFFELSBERG	100	8
	NOBEYAMA	45	3
	GRENADA	30	1.5
	GOTEBORG	21	3
	ATIBAIA	14	5
	FINLAND	14	3
	SPAIN	14	5
	KPNO	12	1.3
	AMHERST	14	3
	CAL TECH	10	1
	BANGALORE	10	1
	HAWAÏ	10	.3

INTERFEROMETERS:

IRAM	3x15m	.7
NOBEYAMA	5x10	1
CAL TECH	3x10	3
BERKELEY	3x6	3

MAJOR ROLE OF SMALL INSTRUMENTS:

COLUMBIA	1.2m	3
BORDEAUX	2.5m	3
TOKYO	1m	3
BERKELEY	6m	3
MWO	5m	1